Analyzing wear condition of wheel on crossing

– A case of Addis Ababa Light Rail Transit line –

Eyob Gachira

A Thesis Submitted to

The School of Civil and Environmental Engineering

Presented in Fulfillment of the Requirements for the Degree of Master of Science (Railway Engineering)

Addis Ababa University
Addis Ababa, Ethiopia
July 2018

Approval sheet

ADDIS ABABBA UNIVERSITY
ADDDIS ABAB INSTITUTE OF THECHNOLOGY (AAIT)
SCHOOL OF CIVIL AND ENVIRONNMTAL ENGINEERING

The undersigned have examined the thesis entitled '**Analyzing Wear Condition Of Wheel On Crossing, Case Of AALRT**' presented by **Eyob Gachira,** a candidate for the degree of **Master of Science** and hereby certify that it is worthy of acceptance.

Mequanent Mulugeta (MSc.)		
Advisor	Signature	Date
Internal Examiner	Signature	Date
External Examiner	Signature	Date
Chair person	Signature	Date

UNDERTAKING

I certify that research work titled "**Analyzing Wear condition Of Wheel on Crossing, Case of AALRT**." is my own work. The work has not been presented elsewhere for assessment. Where material has been used from other sources it has been properly acknowledged / referred.

Eyob Gachira _____ _____.

Signature date

ABSTRACT

The aspects of wear, friction and fatigue are very important in the operation of railways. There exist significant researches that deal with identifying the wear and fatigue mechanisms within wheel-rail contact. Different approaches are necessary to identify different phases on wear and fatigue behavior in wheel-rail contact, eventually making it possible to minimize the problem of unexpected wear and fatigue failure.

Among the numerous components used in the railway industry for the high axle load operation wheels and rails comprise a major source of running expenditure. Wheel wear is one of the common factors that interrupts the vehicle movement and may cause derailment and overturning risk. The evaluation and prediction of wheel wear is a fundamental issue in the railway field, both in terms of vehicle stability and economic cost.

Wheel Wear effect is the main challenge of AALRT which takes more operation and maintenance cost, and also reduces the life of track and vehicles. The study tries to assess whether the crossing alignment is the cause of excessive wheel wears of AALRT, determine wear index and wear rate prediction.

The study has performed the task of determining creepage and creep forces between wheel-rail contacts. It uses the wheel type s1002, and rail USC50 on crossing, by using MBS software. Varied speeds 30kmh, 40 and 50kmh are used, by considering empty and fully loaded vehicle under maximum load of 65 ton. The simulation was made and the results are used to determining wear index by using SIMPACKv8.9 MBS function. Simulation results show that creepage and creep forces are optimum at crossing, which gives the maximum wear index at the points for both fully and empty loaded vehicles. This indicates that crossover is among the causes of wheel wear to wheels of AALRT trains.

Key words: *multi-body system, crossover, wear, creepage, wear index*

ACKNOWLEGMENTS

First of all, I am very delightful to praise the Almighty God who has enabled me to complete my thesis work. Next, I would like to thank my Advisor Mr. Mequanent Mulugeta for his patience, support and guidance. And I would like to express my gratitude to Ethiopian Railway Corporation (ERC) for providing my tuition fee. They gave me valuable information about AALRT track conditions and vehicle specifications as well as provided me the necessaries data and specifications.

I also like to thank the ministry of education (MoE) for giving the opportunity to study my MSc and covering my whole budgets.

Lastly, I extend my sense of gratitude to all my friends who directly or indirectly helped me in my thesis work.

TABLE OF CONTENTS

LIST OF TABLES

LIST OF FIGURES

NOMENCLATURE

The nomenclatures in this report include abbreviations and symbols used in equations, longer naming's, acronyms, representation of quantities and parameters.

Abbreviations

AALRT	*Addis Ababa light rail transit*
CAD	*computer Aided Design*
ERC	*Ethiopian Rail way corporation*
CREC	*China Railway engineering corporation*
DOE	*Design of Experiment*
G2D	*Graph of Two dimension*
MBS	*Multi-body system*
MoE	*Ministry of Education*
WI	*wear index*
2D	*two Dimension*
3D	*Three dimensions*
Wst	*wheel set*

Symbols

A	*contact Area*
A	*work of friction*
d	*distance*
E	*modulus of elasticity*
Ff	*Flange force*
Fn	*Applied load*
G	*shear modulus*
H	*Material hardiness*
I	*unit volume of wear in* mm^2
k	*wear coefficient*
kv, ky	*factor of volume wear*
L	*sliding distance*
N	*Normal force*
P	*pressure in contact patch*

R_{loc}	*is the local rolling radius of the wheel*
rx1	*wheel radius*
ry1	*rail radius*
S	*sliding distance*
T	*Creep Force*
W	*wear rate*
V_{lat}	*lateral velocity of the wheel*
V_{ref}	*reference speed, normally the forward velocity of the Centre of mass*
V_w	*is the forward velocity of the wheel.*
w_{cr}	*critical power*
$w_{friction}$	*friction force performed between wheel and rail*
γ	*longitudinal creepage*
ω	*lateral creepage*
v_w	*Volume of wear*
μF	*Coefficient of friction*
ψ	*Attack angle*
μg	*material loss*
ζ	*full creepage*
ψ	*spin creepage*
υ	*lateral creepage .*
Ωn	*projection of the rotational velocity of the wheel set on the normal to the local rail*
η	*lateral creepage*

CHAPTER 1 INTRODUCTION

1.1 Background

When railway vehicles run on tracks, contact forces are transferred between wheels and rails through the contact patches. These tangential and normal contact forces allow the vehicle to run over the track. Nevertheless the occurrence of sliding can lead to material removal or plastic deformation. Due to these effects the rails and wheels produce a change in geometry of the profiles. This change in the geometry of the profiles is really an important issue since it can change the dynamic behavior of the vehicle. The changes in the changes in geometry and material removal can nowadays be predicted through wear prediction tools. These wear prediction tools are codes developed to know the evolution of the wear. Thus, the evolution of the profiles can be determined without having to run thousands of kilometers and take profile measurements at every specific distance [1]. The wear of wheels and rails has been the main concern in railway business for several decades. With current trends towards increased axle loads and higher speeds, the phenomenon becomes even more accentuated despite significant achievements in material development and vehicle design. The focus on infrastructure maintenance and rolling stock life cycle costs also draw attention to the possibilities of wear control [23].
Railway crossings are the fundamental elements used in railway track structures. It is used in rail transportation to change direction of train and makes transportation system flexibility. There are discontinuities between rails on a crossing. These discontinuities cause a critical stress environment due to higher dynamics going on in the crossing, and result in elevated damages like the mostly observed ones of rolling contact fatigue and wear on wheel and rail. Analyzing and predicting wear is very complex but things can be simplified and researched to get a very good deal of information about wear index determination and wear prediction. Knowing this will enlighten the researchers to take measures to mitigate excessive wear on wheel. The study helps the researches to the most severe cases of wear on crossing, and takes scientific measure to prevent it. The main focus of the current work is on determining the wheel wear index, by altering loads and speeds, and predicting wheel wear. The results of wear analysis wear compared with theoretically expected value of wear index.

1.2 statement of the problem

Among the numerous components used in the railway industry wheels and rails comprises a major source of running expenditure. The wheel-rail interaction is the main technical factor determining design procedure, maintenance and replacement for both vehicle and track. The rail wear is one of the most important cases for reduction of railway track life. In addition to that, the wheel wear is the common factor that interrupts the vehicle movement and may cause derailment and overturning risk. The effect causes re-profiling of wheel and oiling which takes more maintenance cost.

Wheel wear is one of the critical problems of Addis Ababa Light Rail Transit. Large amount of money is spent for oiling or lubrication and maintenance of wheels. Due to this problem, some vehicles are not giving service. The wheels are worn earlier than the expected time. This study tries to assess the cases for wheel wear and also focuses on wear conditions at crossing under **different loads and varying speed**

1.3 Objectives of the study

1.3.1General objectives

The general objective of study is to analyze wheel wear condition of AALRT on crossing by using analytical method and multi-body system software.

1.3.2 Specific objectives

- Determining wheel rail contact points at crossings.
- Wheel wears prediction on crossings.
- Determining wheel wear index under different speed for fully loaded and empty loaded vehicle.
- Identifying possible mitigation methods of wheel wear

1.4 Software for wear analysis

There are modeling and dynamic analyses programs that have received wide acceptance in recent years such as NUCARS***, MEDYANA, VAMPIRE, SIMPACK, ADMAS/RAIL*** and ***GENSIS*** [20].

Although the above programs have different attributes, they were all developed specifically for railway vehicle dynamic modeling and simulations [20]. Each program includes different solution methodology, wheel/rail models, analysis methods and user interface. Among them, SIMPACK- MBS software is accessed. It is a general Multi-Body Simulation Software used to model the dynamic behavior of interconnected rigid or flexible bodies that are subjected to translational, rotational and displacement [20]. The main advantage of this software is that it is adapted to full transient non-linear analyses, even within the acoustic range, being particularly outstanding in transient high frequency analysis; it also used to alkalize material contacts under dynamic impacts [20]. Due to this and others important features, SIMPACK- MBS software package is used to achieve the objective of the study.

1.5 Scopes and limitation

1.5.1 Scope of the study

- This thesis is mainly focused on analyzing wheel wear condition of AALRT on crossing, and predicting wheel wear by using analytical methods with varied speeds and loads. The SIMPACK 8.9, MBS software is used for vehicle modeling and analysis.

1.5.2 The limitations:

- The work is completely based on computer simulation; experimental investigations were not conducted to validate the research.
- It only deals with wheel-rail contact relation, by ignoring the influence of sleeper, ballast and other parameters on dynamics.
- Practically material hardness was not tasted to predict the volume of wheel material removed.

1.6 Organization of the study

The thesis is organized in five chapters. The first chapter is introduction part which states the background of the study, statement of the problems, objectives and scopes and limitations of the research.

Chapter two is about the review of literature for theoretical foundation.

The third chapter discussed about modeling issues of vehicle, methods and the mathematical models to predict wheel wear.

Chapter four contains the results obtained from SIMPACK8.9 multi-body system software and in addition mathematical analyses of wear prediction were done and finally the result was discussed.

The last chapter finally concluded by giving conclusion and forwarding some further works to be made for the better fidelity outcomes we seek for wheel wear prediction and measures to prevent it in railway engineering technology.

CHAPTER 2 LITERATURE REVIEW

2.1 Wear

Wear is the gradual removal of material obtained at contacting surfaces in relative motion. While friction results in important energy losses, wear is associated with increased maintenance costs and costly machine downtime [15].

Wear phenomena are intimately linked to frictional processes. Recall that friction forces are generally the result of two main physical processes: shearing and plugging. If solid surfaces in relative motion are not separated in some way, wear can be expected. Lubricants are used to separate contacting surfaces in relative motion and thus to reduce wear. Lubricants may completely separate the surfaces, as in fluid film lubrication or allow solid-solid contact only at a restricted number of locations (mitigated solid contact) as in boundary lubrication [15].

Wear phenomena are heavily influenced by the fact that most engineering surfaces are rough (and hence surfaces come in contact at single asperities and the real area of contact is usually much smaller than the nominal contact area). Furthermore, wear behavior is also influenced by the presence of adsorbed species and/or surface layers [15].

2.1.1 Wheel wear

Wear affects both wheel and rail. Wheel wear can be separate in several types. Wheel *flange wear*: In this case flange thickness (t_f) is reduced. This is wear type normally produced due to higher creepages and creep forces because of higher coefficient of friction; smaller curve radius and horizontal stiffer wheel set suspension along with longer wheel set base. *Wheel thread wear*; both flange thickness (t_f) and height (h_f) are increased, normally, because of the combination of normal forces with large ordinary or creep forces. Wheel-out of roundness: there are several types such as eccentricity of the wheels due to non-centered position of the wheel with profiling; wheel flat when during braking the wheels are locked and thus do not rotate and waves or corrugations, because of wave around the perimeter due to variation in the wheel rail system. [2]

There are different types of wheel damages. Among this spalling is a well-known rolling contact fatigue damage of the wheel. When a wheel-rail sliding is caused by excessive

braking or acceleration the friction heat is enough to austenite the material near to the contact surface. The crack often initiates in the wheel etching layer and then propagates in to the wheel due to cyclic rolling contact. The crack material breaks away from the wheel and leaves void which is known as **spalling**. This spalling includes two stages. Wheel etching layer from above austenitization temperature and rolling contact fatigue crack with in the material containing wheel etching layer, as consequences, two methods are effective to resist the spalling of railway wheel. The first one is increasing the resistance to wheel etching layer. The other one is delaying the rolling contact failure for wheel steel containing wheel etching layer [13].

2.1.2 Wheel wear at thread

A turnout which includes switches and crossings, are essential components of railway infrastructure that provides flexibility to traffic operation. As the train interring in to turnout there is variation in geometry. The contact point between wheel and rail differs when the vehicle interring in to turnout. At the entrance the contact point moves from stack to switch rail due to the reason that the area of contact differs. This causes an increase of wheel-and rail at the turnout but not the effect of turnout on wheel wear.[13].

2.1.3 Wheel wear due to crossings

Many researchers prove that reduced wear rate of the wheel results increase in wear rate of the rail and vice-versa [13]. But researchers observed that reducing the hardiness of both contact material decreases the wear rate of the materials. The harder material can provide the benefit of reducing the whole system maintenance cost [13].

Crossings are part of turnouts which enables change of direction of moving vehicle. It consists of wing rails, switch machines and movable switch rails. Switches are very important for developing the network of rail line, joining and branching tracks in to differ lines. The components of a switch are very complicated and very expensive. Short line and require high investment and maintenance cost [15].The spring frog provides continuous support for the wheel as it transits through the frog flange way. This frog has movable ring wing rail. The wing rail is held closed by spring assembly. It also has an anchor block thimble and bent joint bar at the toe and to allow the wing rail to pivot. The guard rail pulls the wheels over, forcing wing to open on the diverging side. The wing rail springs closed again after the wheels are through. Spring frogs are supplies as either

right or left hand. To determine the hand of the spring frog, stand at the rigid wing end forcing the frog [14].

2.2 Factors can cause wear

The wear that occurs between wheel and rail while the vehicle is moving depends on different factors, among these, sliding between contact area, normal force, friction coefficient, size and shape of contact area and material properties are common factors highly related to wear. Wear on wheel and rails makes it necessary for the equipment to be replaced when the upper safety limits have been breached and, as a general rule, the vehicle also sustains losses in terms of dynamic performance. Worn profiles tend to be less stable and show lower performance levels when negotiating curved tracks, and this leads to reduced wear index a major factor in the design of railway vehicles [18].

2.3 Wear measurement

It can be seen from published works that number of computational models have been developed for the prediction of wheel wear. These models generally fall in two main categories: Models which assume the material loss is proportional to the frictional energy dissipated in the contact patch (Tγ). Tγ is expressed as the sum of the products of the creepage and creep force for the lateral, longitudinal and spin components, as illustrated below [9].

$$T_\gamma = [T y\gamma\, y] + [T x\gamma\, x] + [M\, z\omega z] \qquad \textbf{(2-1)}$$

Where; T, M = Longitudinal, lateral creep force and spin creep moment components

γ, ω = Longitudinal, lateral and spin creepage components

A number of factors, based on the rate of the Tγ, have been developed to account for the different wear regimes (e.g. mild, severe and catastrophic.) [25]

Sliding models according to Archard where the material loss (Vw) is proportional to the normal force (N) and the sliding distance (s) divided by the material hardness (H), as illustrated below: [24]

$$V_w = K\frac{N*S}{H} \qquad \textbf{(2-2)}$$

The wear coefficient (K) differs depending on the governing wear regime (e.g. mild, severe and catastrophic).

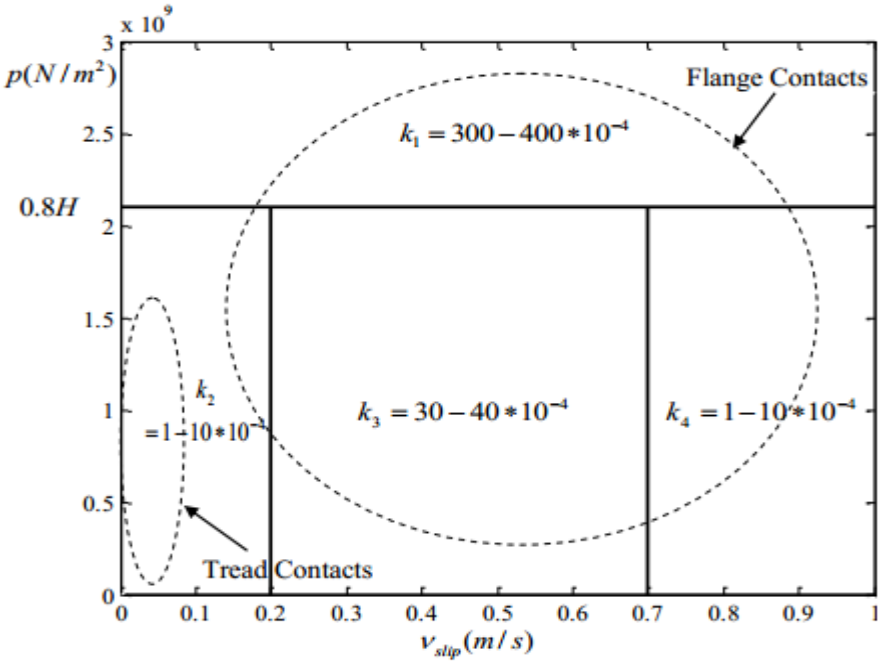

Figure 2-1wear coefficient for typical thread and flange contact depends up on pressure and sliding condition [24]

.

Wear rate measurements are routinely performed using standard or customized friction and wear testing equipment. The same configurations used for friction measurements are also used in wear research. While the occurrence of an initial running-in or breaking-in stage is often detected when measuring wear, experiments tend to focus on the commonly encountered subsequent stage of the process: *steady state wear*.

The amount of material worn in a tribological system is measured in relation to the duration and extent of contact. Specifically, a common measure of wear is the volume of material removed per unit sliding distance. Consider a tribological system where a volume V_w of the softer component of the couple is removed by wear in the same amount of time it takes for the sliding distance to become L. The volume of worn material per unit sliding distance is then $w = V_w/L$. The wear rate thus expressed has units of area and it is often useful to compare the observed values of wear rate against the other most important area measure encountered in friction studies, namely, the real area of contact of the friction couple A_f which, for plastically deforming asperities, is simply given by

$$A_f = \frac{Fn}{H} \qquad \textbf{(2-3)}$$

Where, Fn is the applied load and H is the hardness of the softer component in the friction couple.

The ratio of the wear in units of volume removed per unit sliding distance to the real interfacial area of contact is a meaningful dimensionless quantity useful in wear studies and is called the dimensionless wear coefficient, or simply the wear coefficient, K. From the above, this is defined as

$$K = \frac{Vw/L}{Fn/H} = \frac{W}{Ar} = \frac{W}{Ar} \qquad (2\text{-}\mathbf{4})$$

A couple of useful physical interpretations can be given to the coefficient K. First, since, K is the ratio of two areas, the worn area Aw and the real contact area Ar. One can thus interpret K as the fraction of the real contact area A_f removed by wear. Consider a tribological system consisting of a hard flat surface and a rough surface of a softer material with of identical asperities. Assume the surfaces make contact at N asperities. Hence, the wear coefficient represents the number n of those asperities were conditions are such the conditions that material is torn forming wear debris, i.e[4].

$$K = \frac{Aw}{Ar} = \frac{n}{N} \qquad (\mathbf{2\text{-}5})$$

This interpretation, together with the commonly found low values of K found in practice indicates that while all asperity contacts contribute to friction only a very small fraction of contacts result in wear. Therefore, while friction is dominated by the contact events that occur without damage, wear is dominated by the (small) chance that a particular contact event results in rupture. Note also that the quantity (F_n/H)*L has dimensions of volume. This represents the total volume of the plastically deformed zone underneath the surface of a worn area, V_p following sliding by a distance L [4].

$$\mathrm{K} = \frac{Vw}{Vp} \qquad (\mathbf{2\text{-}6})$$

Therefore, K also represents the proportion of the plastically deformed volume that is removed by the wear process.

At present there are a number of models attempting to quantify the wear index that include some of the abovementioned parameters. In any case, first it is essential to solve the contact problem. This leads to correct location of all contact patches and provides knowledge as to the size and shape of each patch, data which are essential for the application of any wear model [18].

Most used theories in railway dynamics assume that wear is proportional to the energy dissipated within the contact patch, calculated as the scalar product of tangential force on the contact and the value of creepage. Some experiments show that there is a good correlation between the amount of wear measured in wheels and rails and this frictional energy divided by the contact area. The proportionality constant varies depending on wear severity, and the wear rate can be obtained as [18]

$$\frac{T\gamma}{A} < 10.4 N / mm^2 \quad \Rightarrow W = 5.3 \frac{T\gamma}{A} g / m / mm^2 \qquad \textbf{(2-7)}$$

$$10.4 \leq \frac{T\gamma}{A} < 77.2 \ N / mm^2 \quad \Rightarrow W = 55.0 \ g / m / mm^2 \qquad \textbf{(2-8)}$$

$$\frac{T\gamma}{A}{}^3 < 77.2 N / mm^2 \quad \Rightarrow W = 55.0 + 61.9 \left(\frac{T\gamma}{A} - 77.2\right) g/m/ \ mm^2 \qquad \textbf{(2-9)}$$

where, T is creep force at contact patch, v- is creepage, A is the contact area, and W is the wear rate. Creepage is dimensionless, and is calculated as the relative velocity of the contact point of the wheel with respect to the rail (considering rigid bodies) divided by the nominal velocity of the vehicle. For computation of creep forces, it is necessary to use a contact theory to establish the relationship between these tangential forces and the creepages emerging in contact patch [18].

The pattern of wear varies from application to application poor curving vehicle on curvaceous routes will suffer mainly flange wear whereas curving vehicle on relative straight routes will suffer mainly thread wear[18].

Wear characteristics of the wheel influences the life of the wheel; hence it is very important on the view point of economy means maintenance cost. The major factor that influences the wear characteristic from material perspective is carbon content of the material. The higher carbon content the higher the material to resist the wear. But, from track component perspective curve radius, vehicle configuration, suspension design, wheel profile, rail profile, wheel-rail friction, cant deficiency, traction and braking force, track geometric quality, are the primaries which causes rolling contact fatigue, wear [15].

2.4 Stages of wear

Under normal mechanical and practical procedures, the wear-rate normally changes through three different stages [7]

- Primary stage or early run-in period, where surfaces adapt to each other and the wear-rate might vary between high and low.

- Secondary stage or mid-age process, where a steady rate of ageing is in motion. Most of the components operational life is comprised in this stage.
- Tertiary stage or old-age period, where the components are subjected to rapid failure due to a high rate of ageing.

The secondary stage is shortened with increasing severity of environmental conditions such as higher temperatures, strain rates, stress and sliding velocity etc. strain rates, stress and sliding velocities etc. Note that, wear rate is strongly influenced by the operating conditions. Specifically, normal loads and sliding speeds play a pivotal role in determining wear rate. In addition, tribo-chemical reaction is also important in order to understand the wear behavior. Different oxide layers are developed during the sliding motion. The layers are originated from complex interaction among surface, lubricants, and environmental molecules. In general, a single plot, namely wear map demonstrating wear rate under different loading condition is used for operation. This graph also represents dominating wear modes under different loading conditions [7].

In explicit wear tests simulating industrial conditions between metallic surfaces, there are no clear chronological distinction between different wear-stages due to big overlaps and symbiotic relations between various friction mechanisms. Surface engineering and treatments are used to minimize wear and extend the components working life [7].

2.5 Wear prediction

The core of wear prediction tool is wear computation, computing the amount of war material from worn surface starting from MBS dynamic result. It can be considered to be divided in to three parts [21].

1. Contact model
2. Wear function
3. wear distribution

The contact model processes the dynamic analysis result to obtain the wheel-rail contact parameter. The war function used those contact parameters as impute to compute the quality of worn materials along the wheel profile [21].

Considering the contact model, two alternative materials have been implemented, global or local depending on the way they solve the wheel-contact problem. In the global approach the contact parameters are obtained by studying the contact problem on the whole wear –rail contact patches, considering the mean value of normal and tangential

forces. In the local method, the contact problem is studied by dividing the wheel rail contact area in to small cells and evaluating the contact parameters individually for each cell. The war function relate the energy dissipate in the wheel-rail contact patches with the amount of worn material to be removed. In general, these wear laws use asset of contact parameters. Namely the normal and tangential forces and the relative slip velocity (creepage) as an impute to compute the wear **[21].**

This method relates the wear rate representing the weight of loss material (μg), per distance rolled (m) per contact area A (mm^2) to the product (Tγ) (the T is tangential contact force γ is global creepage force this formation is based on twin disc experimental data acquired from S1002 wheel type with flange angle 70 degree, 21.21mm flange thickness and 50 Kg/m U71Mn (Tensile strength=880Mpa from Chinese standard. The method has identified three regimes, mild serve and catastrophic for the contact between wheel and rail materials [21].

Table 2-1: equation for wear function, [21].

Wear regime	**Wear range Tγ/A[N/ Tγ)**	**Wear rate μg/m/mm^2**
Mild	Tγ/A < 10.4	5.3* Tγ/A
Serve	10.4 < Tγ/A≤77.2	53.3
Catastrophic	Tγ/A ≥ 77.3	60.9* Tγ/A

2.5.1 Wheel prediction Model

Ward, Lewis and dwyer Joysce uses rail interface to calculate contact position, the force and slip using wheel and rail profiles, wheel set design, friction coefficient and material properties. Based on an energy approach it used wear coefficient as an input. The contact between wheel and rail is assumed to be an ellipse [4].

$$\text{Wear rate } (\mu g/m/mm^2) = \frac{ke * T * v}{A} \qquad \textbf{(2-10)}$$

Where, k_e is the wear coefficient in (μg/Nm), T is tractive force (N), v is total creepage between wheel and rail ,A is contact area in mm^2

Klaker and Li**:** [28] in wear calculation method, the wheel- rail contact is calculated by the FASTISM method while the pressure of contact and the area of contact are calculated according to the Hertz's theory. The method did not take the flange wear in to account because they taught that hertz's theory is not applicable for sever conditions. The material removed during the work is characterized through the work that is performed and the contact, C, is obtained by some measures performed by Lahana [4].

$$\text{Mass } (\mu g) = C\ (\mu g/N/mm) * W_{frictional} \quad \textbf{(2-11)}$$

$W_{frictional}$, the friction force performed through the contact between wheel and rail. Taking in to account the above equation

$$V_{wear} = k1 \frac{d*T}{H} = k_w * W_{friction} \quad \textbf{(2-12)}$$

Where: k_1, is coefficient, d(m) is sliding distance, T(N) is friction force such as, $W_{Friction}$=Td, H is hardness of material and k_w is friction coefficient depends on several parameters, material property, lubrication property, force and pressure in the contact.

2.6 Models of wear intensity

2.6.1 Archard model

The model is based on the hypothesis of the linear dependency between volume wear *I* and the work of creep force A: [23]

$$I = k_v A \quad \textbf{(2-13)}$$

Where:

I is volume wear mm^3

Kv-is factor of volume wear m^3/J

A - Is the work of friction in J

Table 2-2: typical value of dimensionless wear coefficient for various materials against tool steal sliding in dry un lubricated, pin-on disc test in air.[23]

Material	K
Mild steel (on mild steel)	7×10^{-3}
α/β brass	6×10^{-4}
PTFE	2.5×10^{-5}
Copper–beryllium	3.7×10^{-5}
Hard tool steel	1.3×10^{-4}
Ferritic stainless steel	1.7×10^{-5}
Polythene	1.3×10^{-7}
PMMA	7×10^{-6}

Archard model, Archard's wears equation

$$V_w = K \frac{N*S}{H} \quad \textbf{(2-14)}$$

$$\Delta S = k\frac{P*\Delta S}{\Delta H} \quad \textbf{(2-15)}$$

Where: Vw-volume of wear (m^3) S- Sliding distance (m)

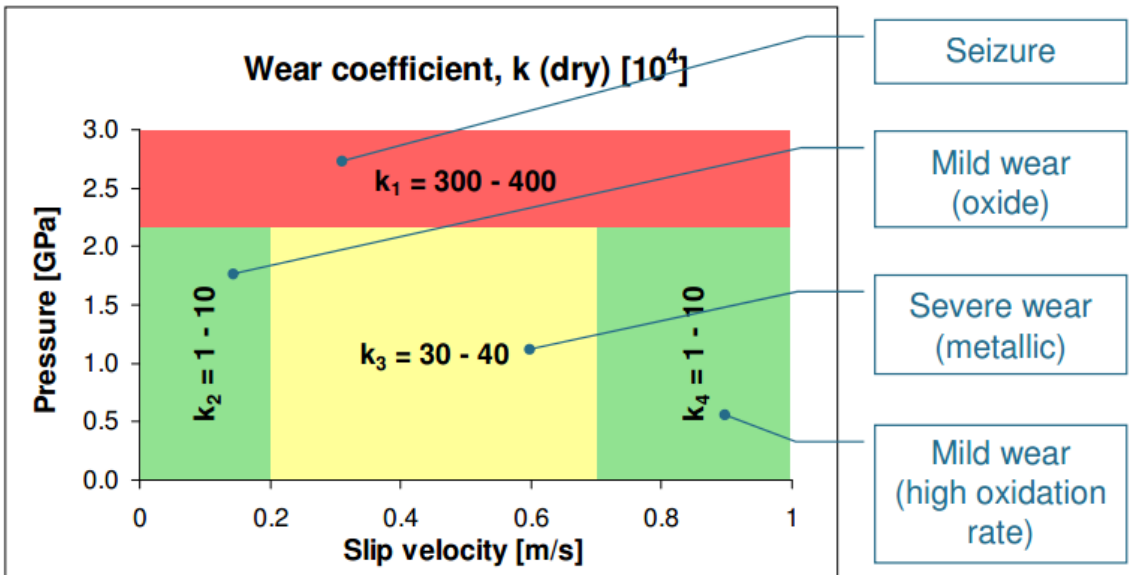

Figure 2-2wear map of wear coefficient [23]

2.6.2 Specht model

This model is also used the linear dependency between the volume wear and the work, but it is assumed that exist two areas within the contact patch: the area of moderate and intense wear with different value of wear coefficient: [23].

$$I = k\nu A \qquad w < wcr \quad \textbf{(2-16)}$$

$$I = k\nu\alpha A \qquad w \geq wcr \quad \textbf{(2-17)}$$

Where:

I -is volume wear mm^3

Kv-is factor of volume wear m^3/J

A-Is the work of friction in J s friction power W/m^2

Wcr –critcal power W/m^2,*α- jump coefficient*

2.6.3 VNIIZTH model

It considers a geometry dependent spin in each element of the contact area to account for a varying contact angle within the contact patch. .

$$I = k\xi^2 * p \quad \textbf{(2-17)}$$

k- Wear coefficient

ξ –full creepage

P-pressure in contact patch

In the first and second model (Archard model and Specht models) the volume mass wear is proportional to the work of coefficient. Choice of wear factor is difficult problem depending on the material properties, contact condition and etc. Experiments show that the mass wear factor lays on the interval 10^{-4}-10^{-2} mg/J. According to the value of mass wear factor is km = (1.18-2.4) *10^{-3} mg/J for stiff wear condition like Gottard line [2].

$$K\upsilon=\frac{Km}{\rho} \quad \textbf{(2-18)}$$

Spcht model supposes to use km=7.8*10^{-4} mg/J for moderate area that is k_v=1*10^{-13} mg/J for steel weigh 7800kg/m^3 density in the intense wear area 7.8*10^{-3} mg/J and the critical friction power 4 W/mm^2 [4].

The royal institute of technology (KTH) developed the following wear model based on Archard model. The volume of worn material is written as:

$$V=K_A\frac{PS}{H} \quad \textbf{(2-19)}$$

Where:

V-volume of worn in (mm^3)
S-sliding distance in mm
H-hardness of soften material in (N/mm^2)
K_A-wear coefficient
P-contact pressure

2.6.4 USFD model

The University of Sheffield (USFD) developed the following wear model. The wear functions developed by the USFD related to the wear rate, which expressed the weight of the lost material (µg) per distance rolled (m) per contact area (mm^2) to wear index as follow:

$$\text{Wear rate} = K\frac{T\gamma}{A} \quad \textbf{(2-20)}$$

Where:

K-wear coefficient
T-creep force
γ –slip
A-contact area

2.7 Creep force

Creep force: When a railway wheel deviates from pure rolling, that is during acceleration, braking or curving or when subject to lateral forces through the suspension,

forces tangential to the normal force are transmitted to the rail at the contact patch. These are called creep forces and are due to micro slippage or creepage in the area of contact [19].

In a railway wheel, the creepage can be calculated from the attitude of the wheel set and the resulting creep forces may then be evaluated. The relationship between creepage and creep force has been studied thoroughly by Kalker and his equations are used in almost all simulations [19].

For small creepages the creepage-creep force relationship is linear and the linear 'creep coefficients' can be calculated based on contact patch geometry and material properties. At high creepages (full slip) the creep force is limited by the product of the normal force and the coefficient of friction [19].

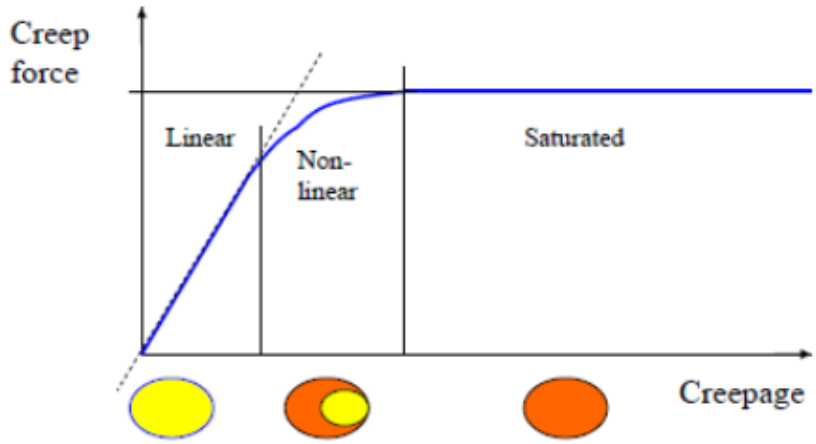

Figure 2-3 Kalker's linear theory versus Carter's creep curve (bold blue line) [10]

$$Vx = \frac{Vw - \omega Rloc}{Vref} \quad (2\text{-}21)$$

$$Vy = \frac{Vlat}{Vref} \quad (2\text{-}22)$$

$$\psi = \frac{\Omega n}{Vref} \quad (2\text{-}23)$$

2.8 Creepage

Creepage is the relative slip between the wheel and the rail. The longitudinal (η), lateral (ν) and spin (ψ) creepage can be defined as follows:

Longitudinal creepage: When the wheelset is rolling freely without traction or breaking, due to the conicity, the two different rolling radius generates the two opposite forces fx and –fx. The creepage due the forces is longitudinal creepage [5].

Lateral creepage: The lateral creepage in quasi-static conditions, with small creepages, is simply the yaw angle common to the two wheels [5].

Spin creepage: It is the difference in angular velocity of wheel within contact patch [5].

2.9 Wear index

When the optimization problem has been solved, the dynamic performance of the vehicle with the obtained wheel profile has to be checked. The tramcar was modeled in the ADAMS/Rail computational package. Standard ADAMS/Rail function has been used for calculation of the wear index. The wear index is calculated as follows (taken from the English Normative (British Rail)). [16]. Wheel-rail contact forces are predicted for the chosen route conditions using vehicle dynamics simulations. These wheel-rail forces are then post-processed to predict the formation of wear on the wheel using a combination of the Archard and frictional energy damage models. Models which assume the material loss is proportional to the frictional energy dissipated in the contact patch. Wear index is expressed as the sum of the products of the creepage and creep force for the lateral, longitudinal, as illustrated below [7].

.

$$W = F_1 \cdot \xi + F_2 \cdot \eta \qquad \textbf{(2-24)}$$

CHAPTER 3 METHODS AND SIMULATION

3.1 Methods

Multi-body system simulation is used to predict and optimize the behavior of any type of multi-body systems by solving dynamic equations. Multi body system is a wide range of system including machines, robots, vehicles, rigid body elements etc. usually during modeling multi-body system the bodies or elements are linked by joints which allow motions and restrict the others. The body themselves can be rigid or flexible. The movement within its degree of freedom is defined by the force or torque element using an arbitrary force or torque law. The system is completed by excitation element and sensor for measuring the desired outputs. In describing the kinematic behavior, the motion or the position of kinematic behavior is studied with respect to kinematic joints. Dynamic problems describe the motion of the system due to applied force and inertia characteristics of the bodies; mass, center of gravity and moment of inertia.

The computational tools developed here to determine wear index of railway wheels consists of using commercial multi-body software (MBS) to study the railway dynamics problem. It uses the purpose built code to manage pre and post processing data in order to compute the wear index. According to this strategy an initial wear profile is provided and the software runs a simulation by using necessary data from the dynamic analysis results. From simulation results wear rate is calculated.

In real situation, many vehicles are operated on different track geometry. Therefore, prediction of wear evolution of the wheel of railway vehicle in different track geometries and other factors has to be considered to wear studies. In this thesis, the geometric components of the track such as crossing and straight alignments are considered to calculate wheel wear under different load and speed operations.

3.1.1 The general over view of wear prediction tools

The following steps used during the analysis of wheel wear.

1. Prepare the input data of computation
2. Prepare the wheel-rail contact data file
3. Run the multi-body dynamic analysis
4. Read the multi-body dynamic analysis output: creepage and creep forces
5. Compute the wear indices, wear rate
6. By varying loads and speeds repeat the same procedure

3.2 Simulation

3.2.1. Multi-body system

Multi-body simulation (MBS) is a method of numerical simulation in which multi-body systems are composed of various rigid or elastic bodies. Connections between the bodies can be modeled with kinematic constraints (such as joints) or force elements (such as spring dampers). Unilateral constraints and Coulomb-friction can also be used to model frictional contacts between bodies. Multi-body simulation is a useful tool for conducting motion analysis. It is often used during product development to evaluate characteristics of comfort, safety, and performance [22]. For example; multi-body simulation has been widely used since the 1990s as a component of automotive suspension design. It can also be used to study issues of biomechanics, with applications including sports medicine, osteopathy, and human-machine interaction [6].

The heart of any multi-body simulation software program is the solver. The solver is a set of computation algorithms that solve equations of motion. Types of components that can be studied through multi-body simulation range from electronic control systems to noise, vibration and harshness [11].Complex models such as engines are composed of individually designed components, e.g. pistons/crankshafts [25].

The MBS process often can be divided in 5 main activities. The first activity of the MBS process chain is the “3D CAD master model”, in which product developers, designers and engineers are using the CAD system to generate a CAD model and its assembly structure related to given specifications. This 3D CAD master model is converted during the activity “Data transfer” to the MBS input data formats i.e. STEP. The “MBS Modeling” is the most complex activity in the process chain. Following rules and experiences, the 3D model in MBS format, multiple boundaries, kinematics, forces, moments or degrees of freedom are used as input to generate the MBS model. Engineers

have to use MBS software and their knowledge and skills in the field of engineering mechanics and machine dynamics to build the MBS model including joints and links. The generated MBS model is used during the next activity "Simulation". Simulations, which are specified by time increments and boundaries like starting conditions, are run by MBS Software i.e. MSC ADAMS. The last activity is the "Analysis and evaluation". Engineers use case-dependent directives to analyze and evaluate moving paths, speeds, accelerations, forces or moments. The results are used to enable releases or to improve the MBS model, in case the results are insufficient. One of the most important benefits of the MBS process chain is the usability of the results to optimize the 3D CAD master model components. Due to the fact that the process chain enables the optimization of component design, the resulting loops can be used to achieve a high level of design and MBS model optimization in an iterative process [14].

3.2.2 The process used during simulation

Based on this paper, the following process is explained separately:

A. The **pre-processing** module is used for building the MBS together with its corresponding3D geometry. Some of the available features from this menu are as follows; Open Model, Model set up, MBS Define body, MBS Define Joint, Define constraints, Force Elements, Define sensor, vehicle global, track definition, information, and element menu and so on. In this MBS model window, each body mass, center of mass, movement of inertia, marker point, joint state, DOF, force element, force type, speed, track and wheel type, track irregularities and other important criteria's were justified.

B. **The processing** module mostly contains calculations and parameter variation process to allow the user to configure and perform different calculations; Assemble System, Nominal Force Parameters, Eigen values, Time Integration and Measurements; perform time domain, kinematic, Eigen frequency, critical.

C. **The post-processing** step deals with the final result plotting and extracted data from the simulation. The SIMPACK program offers detailed results for each body forming the multi-body model in the railway vehicle. The output shows the Para variation time domain 2D plots, G2D plots and state plot.

SIMPACK allows the results of calculations to be animated in 3D in either the SIMPACK Post Processor or the 3D Model Setup window.

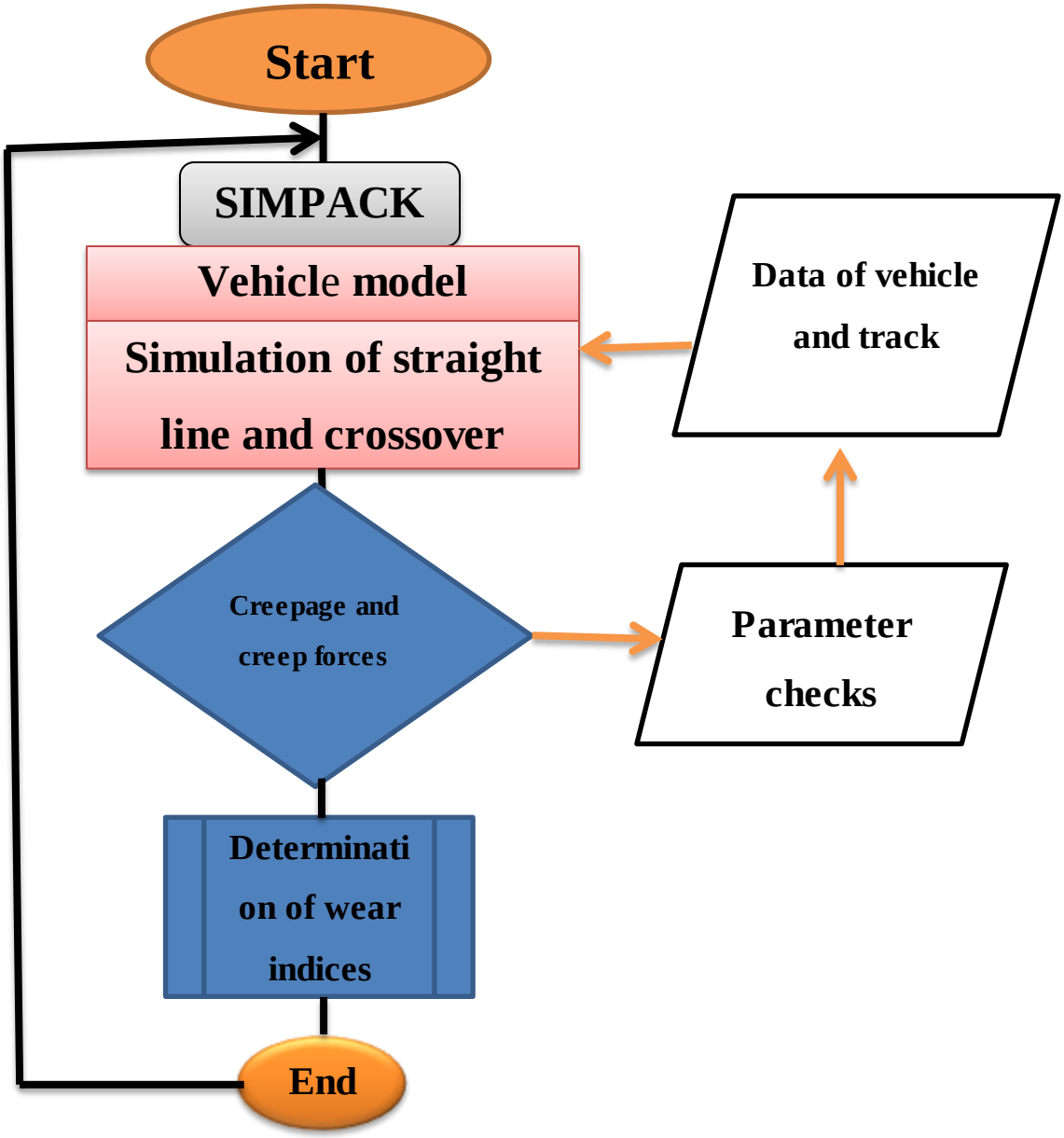

Figure 3-1 detail configuration process to determine wear index [20].

3.2.3 Parameter identifications

Table 3-1: Vehicle geometric data of LRT

No	Basic parameter	Value
1	Track gauge	1.435m
2	Bogie base	10.4m
3	Wheel set base for motor bogie	1.9m
4	Wheel set base for trailer bogie	1.8m
5	Bogie mass for motor bogie	5120kg
6	Bogie mass for trailer bogie	3120kg
7	Car body A or B mass (front and rear car body)	17500kg
8	Car body movement of inertia along x direction	4375
9	Car body movement of inertia along y direction	8750
10	Car body movement of inertia along z direction	8750
11	Car body B mass	12325
12	Car B movement of inertia along x direction	3081.25
13	Car B movement of inertia along y direction	6162.5
14	Car B movement of inertia along z direction	6162.5
15	Bogie movement of inertia along x direction	1250
16	Bogie movement of inertia along y direction	1870
17	Bogie movement of inertia along z direction	2182
18	Front and rear car body length	11.800m
19	Middle car body length	3.600m
20	Height car body including pantograph	3.750m
21	Width of car body	2.650m
22	Vertical mass center of Car body	-0.9m
23	Vertical mass center of bogie	-0.528m
24	Primary spring stiffness along x/y/z	5.8*10^5/5.8*10^5/1.45*10^6
25	Primary damping ration along z	1.25*10^5
26	Secondary spring stiffness value along x/y/z	3*10^5/3.5*10^5/5x 105
27	Secondary damper x/y/z	0/2.0 x 105/4*10^5
28	Minimum radius of vertical curve	1000m
29	Minimum radius of horizontal curve	50m

Table 3-2 dynamic simulation conditions [10] .

Dynamic simulation condition	
Vehicle weight	Maximum pick hour load
Wheel type	S1002 wheel type with flange angle 70 degree, 21.21mm flange thickness
Rail type	UIC 50 rail type with track irregularity
Operating speed	Design speed (40km/h) for straight track
	35km/h for crossover track with curve radius R50m
Operating condition	Under dry weather condition
Track condition	Stadium (cross over section)
	Lideta (cross over section)

Table 3-3 Load parameters [21]

Working condition	Seating capacity	Standing capacity	Total capacity (person)	Total weight (t)
W_o	0	0	0	44
W_1	65	0	65	47.9
W_2	65	189	254	59.2
W_3	65	252	317	63

3.2.4 Crossing

Crossings are track components that divide the track in to two; sometimes in to three if the train passes from one track to another. It is used to guide the train to change the direction while traveling.

Crossing features a straight section called the through route and a curved deviating part called the diverging route. The front of the turnout is defined as the start of the deviating curve in the switch panel. The switching function is realized by switching machines or actuators that position the switch rails according to the desired traffic route. The closure panel connects the switch and crossing panels, whereas the crossing panel allows for wheels to travel along both intersecting paths. Opposite to the crossing, and next to the

adjacent through (stock) rails, are the check rails that enforce a constraint on the lateral position of passing wheel-sets. This is to avoid interference contact between wheel and crossing nose [8].

There are two different types of turnout entry: tangential entry and radial entry. It describes the track route before the switch. In the tangential entry the switch tongue builds up as a tangent, parallel to the straight track before the radius of the diverging track begins. And in the radial entry the switch rail starts to build up within the curvature. High lateral contact forces are present between the wheel and rail as the train negotiates the diverging track [3]. Cross over dimensions used during modeling are from chines standards, table 3-4.

The variations and discontinuities in rail profiles, present in the turnout to achieve the function of the switch and crossing, result in an increased dynamic loading during wheel passage and thus increased degradation of these components compared to regular track. Further, turnouts are often built without transition curves, causing high vehicle jerk (time derivative of lateral vehicle acceleration) at entry and exit of the diverging route. Due to the planar nature of a turnout, track inclination (cant) to compensate for the lateral acceleration is not possible [8].

Because it is impractical to plane down a rail to give a tangential entry to the turnout direction an entry angle is unavoidable. This is followed by the plane radius, which is effective over the length of switch rail which is planed away, i.e. that part of the switch rail which is touching the stock rail. The radius then changes to the switch radius which is a tangential curve to the through straight track, and finally onto the turnout radius is which is chosen to give a crossing angle within a range of standard values and is often equal to the switch radius. The radius of the turnout curve can then begin [5].

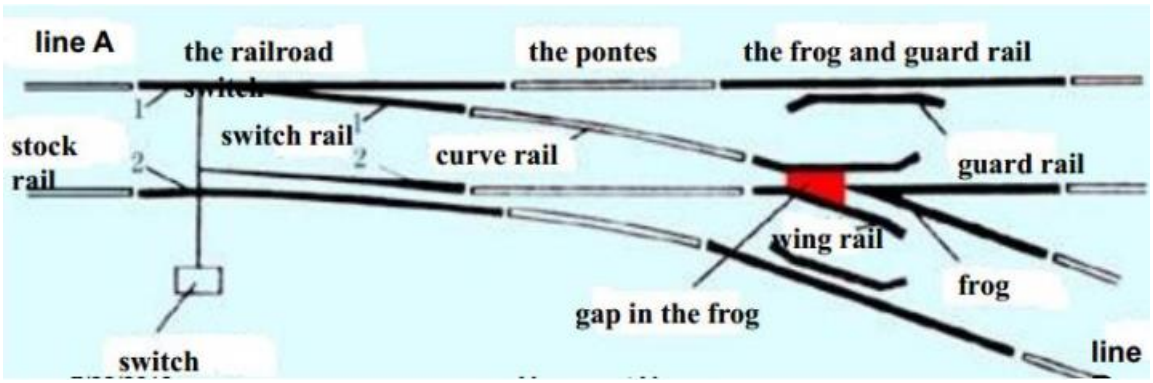

Figure 3-2 simple turnout detail [8].

Table 3-4 Crossover Dimensions [10]

Frog angle (deg.)	Lead curve central radius (m)	Distance between beginning and center of turnout (m)	Distance from center of turnout to heel of frog (m)	Total turnout length (m)	Permissible speed (Km/h)
$6^0$20'25"	180	13.839	15.009	28.848	30

3.2.5 3D modeling of passenger rail vehicle

After modeling wheels and axles, then, modeling the axle boxes, primary suspension components, and bogie frames by using graphical user interface window was made. The primary suspension force elements start from wheel set axle box to bogie frame and the force type is spring damper parallel component forces.

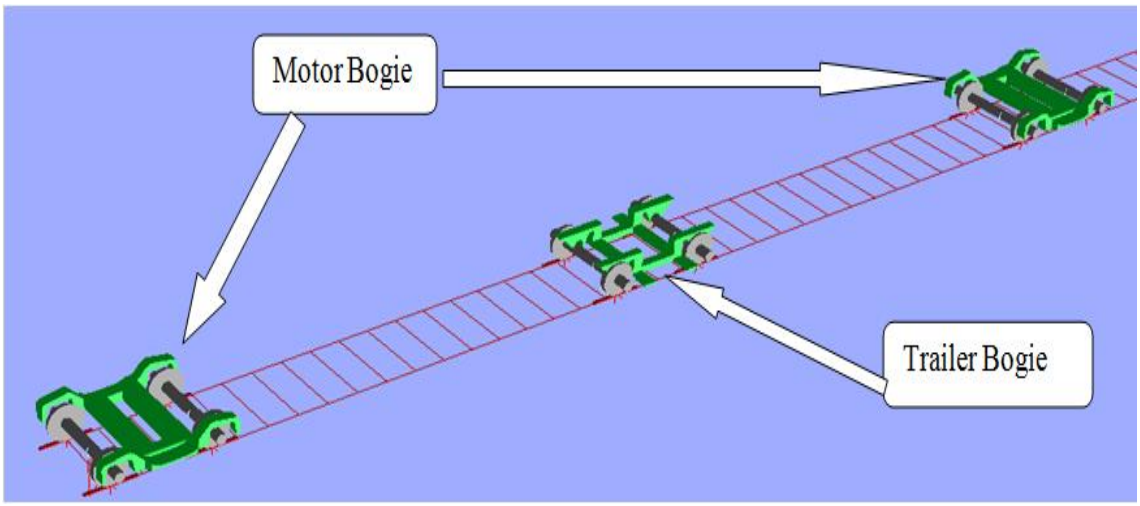

Figure 3-3 Wheel sets, axle boxes and bogie frames

Figure 3-4 shows that, the two the bogie frame is the intermediate component between wheel set and car body module. This system connects to the wheel set and car body by force element which means primary suspension connects bogie frame to wheel sets and secondary suspension connects car body to bogie frames. This frame has many marker points and force elements to connect different components like wheel set to bogie frame, bogie frame to car body in longitudinal, lateral and vertical point of contact, stopper, traction, weight balance and etc.Side lower fixed articulations, upper flexible and free

articulation including middle car body-B and middle bogie frame and also the lower articulation damping components.

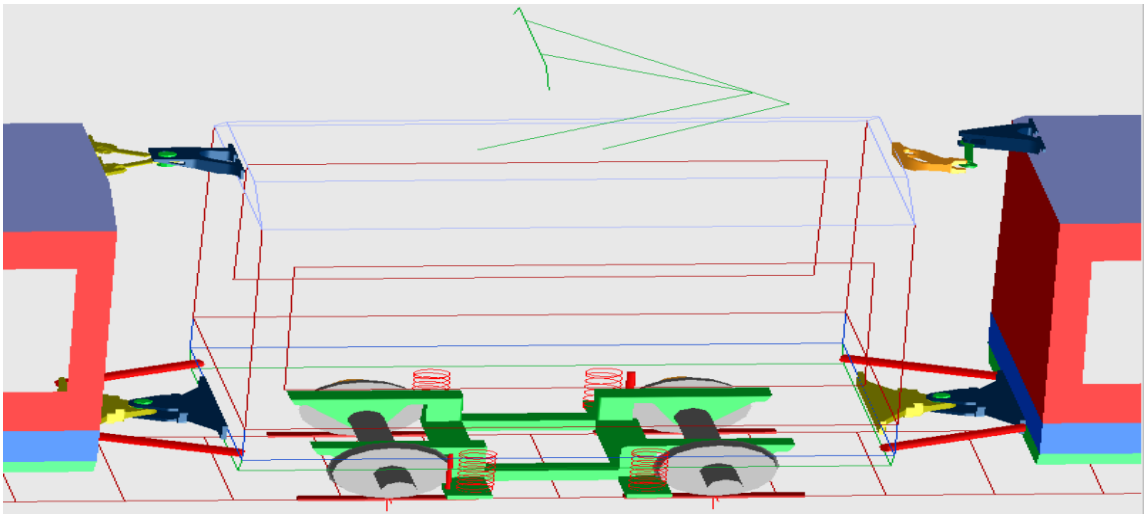

Figure 3-4 two side lower and upper articulations and car body-B

The 3D assembled articulated passenger vehicle including some of marker points and corresponding force elements shown in figure 3-5.

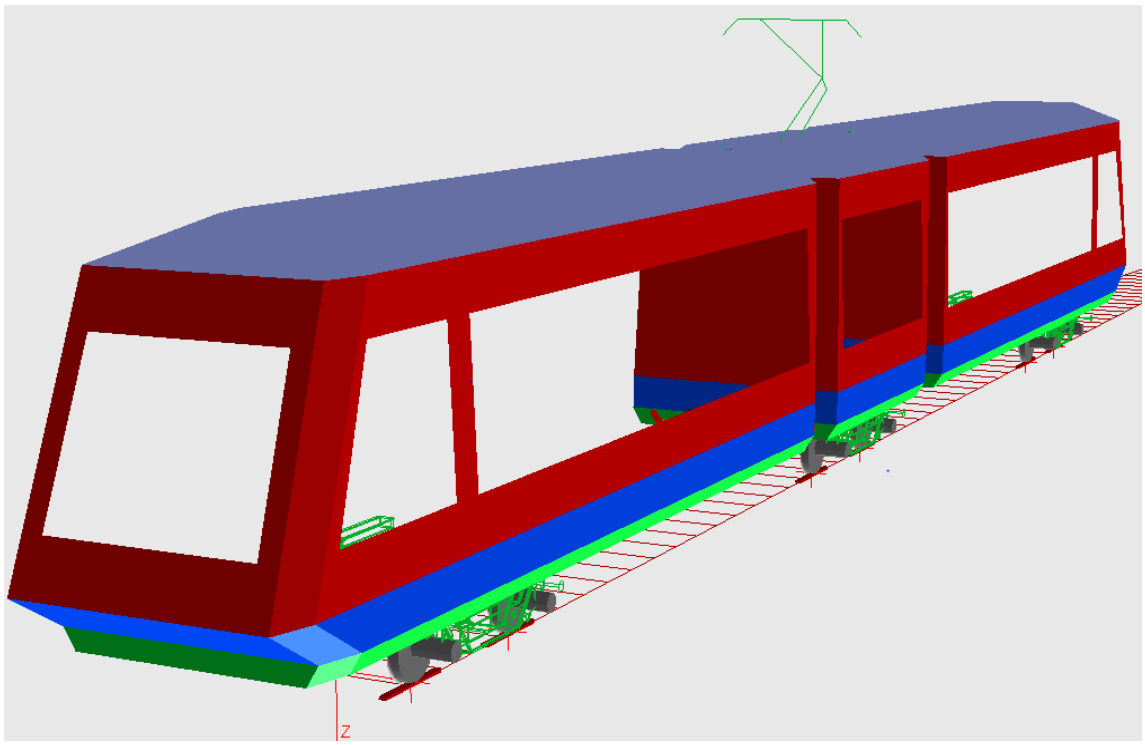

Figure 3-5 Model of car body.

The assembled vehicle body contains all the necessary components, marker points, force elements, the wheel sets, the axle boxes, the three bogies, the three car body modules, the

lower and upper articulation components, the primary and secondary longitudinal, lateral and vertical suspensions, dampers and other important components shown in the figure 3-5 in assembled form. To see all components, see the side view, front view and top view in assembled form in the figure 3-6.

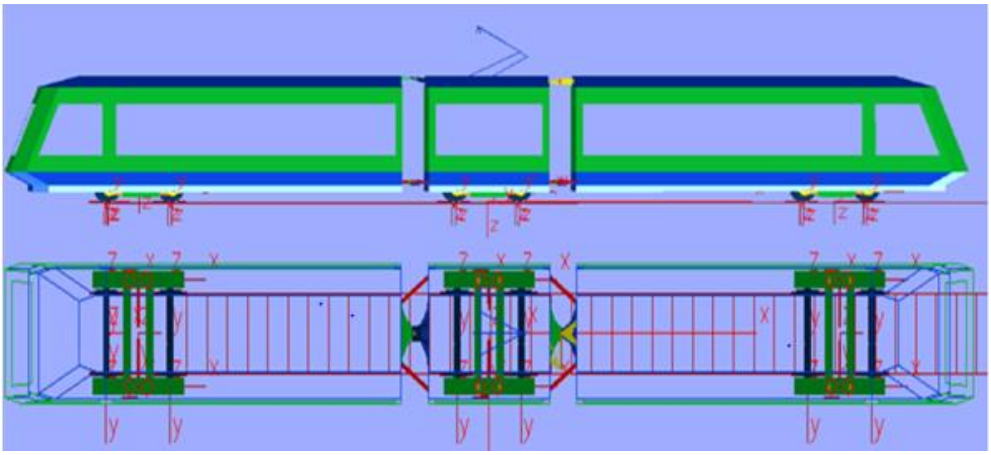

Figure 3-6 Front, side and top view of car body.

According to track topology, there are different types of tracks such as straight track, constant curve, curve entry, curve passing, sign change curve and crossing. For this paper, straight track and sign change curve at super elevated track at different simulation parameter was studied.

Figu

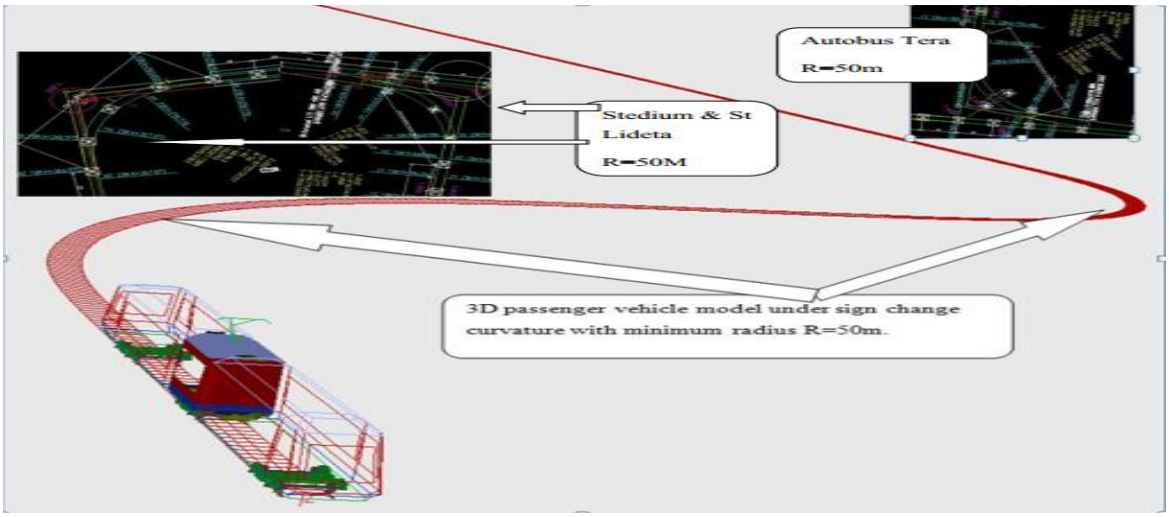

Figure 3-7 3D model vehicles on track

CHAPTER 4 RESULTS AND DISCUSSIONS

4.1 Introduction

This chapter presents the core points of the report, apart from the previous section being the root for this section, in that, simulation and the analysis of the simulation runs were conducted, in order to find wear index and predict wear. The mathematical calculation was made to determine the wear rate, which is directly proportional to traveled mileage, which can be used by other researches. By testing material hardiness any researcher can calculate the material removal at certain travelled distance, which is not included here due to certain limitations. And finally summary has been given about the discussions made on this section.

In all presented cases, the tram simulations has been performed for the 30m straight track with 60m crossover distance and 30m intermediate length with default #9 frogs. The total animation length is 1000m. The vehicle allowed traveling with minimum speed 30kmh and max 70kmh.

4.2 Results

This section contains the analyzed results in 2D plots that are explained and discussed in the next section. All the analyzed results related to our main objectives, wear rate investigation at crossing, such as: creep forces, creepage, wheel-rail contact force, wear index and wear rate prediction are included.

4.2.1 Creepage

Table 4-1Max.and Min. values of lat. creepage

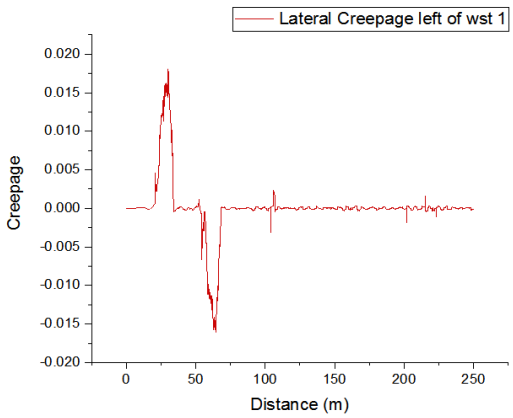

		Index	Value
creepage	Highest	364	0.01808
		362	0.01789
		366	0.01772
		365	0.01748
		363	0.01685
	Lowest	775	-0.01606
		777	-0.01581
		770	-0.01578
		757	-0.01576
		774	-0.01574

Figure 4-1 lateral creepage force left of wst 1

Table 4-2 Max. and Min. values of longi. creepage

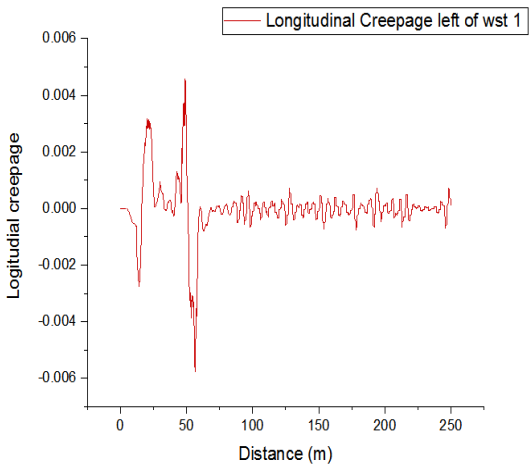

		Index	Value
creepage	Highest	340	0.00409
		344	0.00408
		339	0.00405
		343	0.00399
		342	0.0039
	Lowest	736	-0.00325
		731	-0.0031
		730	-0.00302
		729	-0.00301
		718	-0.00301

Figure 4-2 longitudinal creepage left of wst 1

From figures 4-1 and 4-2 we undertand that the Oscillations of the slender switch blade are greater than those of normal track. Due to this movement threre is abrupt change of creepage when the vehicle moves from switch rail to stock rail. longitudinallty threre is high index of creepage relative to lateral creepage.the index values. From tables 4-1 and 4-2 the raw under highest values indicated the right side from the center the lowest for left sides from the center. index from the table index the point of index values location .

4.2.2 Creep forces

Table 4-3 Max. and min. values of lat. Creep force

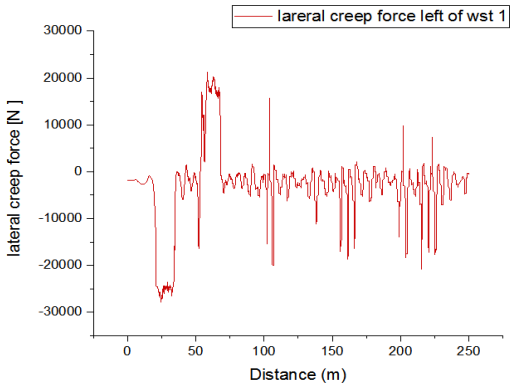

		Index	Value
creep force	Highest	705	21286.4
		704	21217.3
		702	20914
		703	20838.8
		706	20454.2
	Lowest	295	-27824.9
		296	-27743.7
		297	-27514.7
		298	-27374.4
		294	-27279.8

Figure 4-3 lateral creep force left of wst 1

Table 4-4 Max. and Min. values of lat. creepage

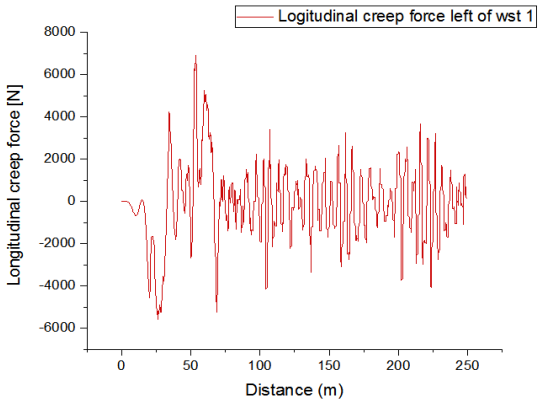

		Index	Value
creep force	Highest	167	7993.53
		166	7984.27
		168	7973.76
		165	7954.27
		169	7917.48
	Lowest	513	-7996.98
		512	-7963.73
		514	-7917.9
		511	-7733.42
		515	-7721.13

Figure 4-4 longitudinal creep force left of wst 1

From tables 4-3 and 4-4 wheels creeps more laterally at crossing due to high creep force. This indicates that there is gauge variation throughout the length of track which interrupts the movement of vehicle. As noted from the above figures 4-3 and 4-4 the point at interval 50 up to 60 meter s highly influenced by the tangential force (creep force) and sliding distance (creep) occurring within the wheel-rail contact. Traction and creepage effects directly relate to the magnitude of creep forces and slip acting at the wheel/rail interface. The level of traction and creepage is highly influenced by the traction demand from the vehicle, friction conditions and geometric dimension.

4.2.3 Wheelset contact geometry

When two bodies (wheel and rail) comes into contact stresses and deformations develop.

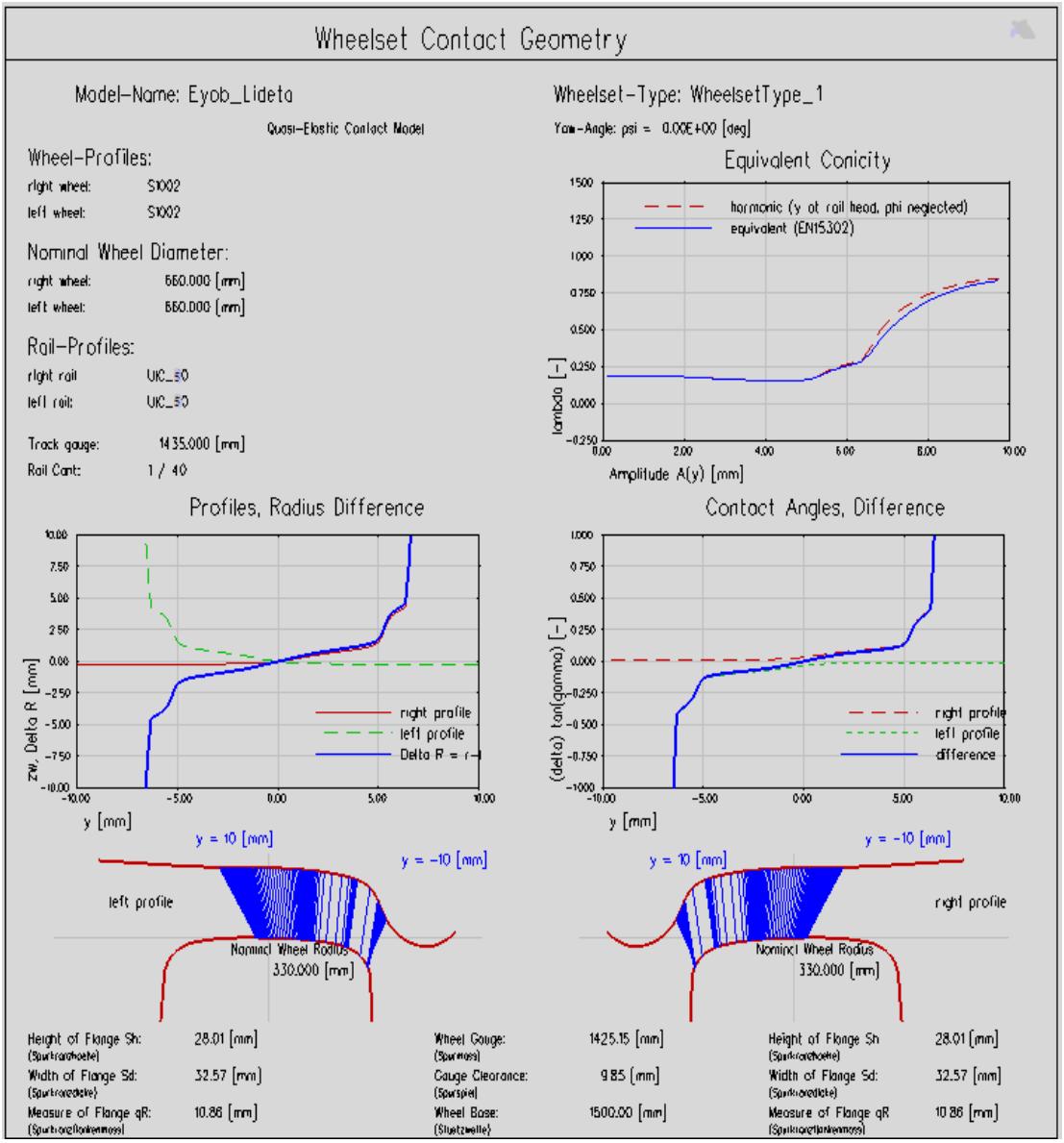

Figure 4-5 wheel-rail contact

From figure 4-5 Lateral contact point location on the wheel with the relative lateral shift y (-10) between wheel and rail is not varied. This indicates there is no sinusoidal movement. The locations of the contact points and the corresponding contact angles determine the locations and the orientations of the contact forces, respectively. Contact forces acting in the point of contact are subdivided into normal forces and tangential friction (creep) forces. The default assumption of just one point of contact per wheel can be replaced by a multiple contact model, allowing up to three different points of contact per wheel: one on the tread, one on the flange and a third one again on the flange or on

the back of the wheel. There is high contact per wheel on the flange of wheel; the wheel wears more on flange. Refer **Appendix B.**

4.2.4 Wheel-rail contact force SIMPACK simulation results

Table 4-5wheel-rail contact force of wst 1,3 and 5 respectively

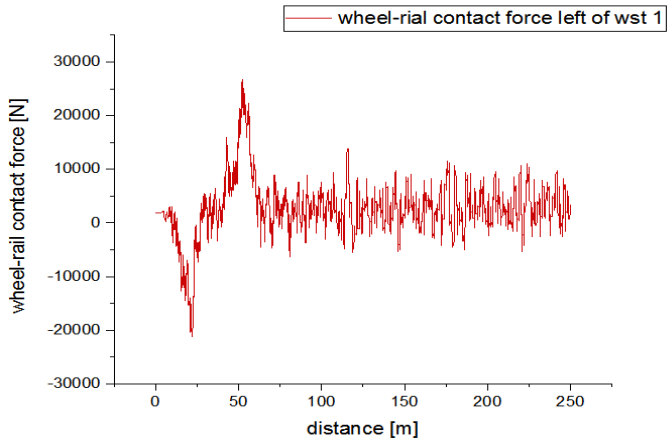

		Index	Value
wheel-rail contact force	Highest	684	30274.8
		705	30128.1
		693	29896.5
		688	29589.2
		704	29278.3
	Lowest	202	-42116.5
		205	-41804
		204	-41737.1
		203	-41662.1
		201	-41232.8

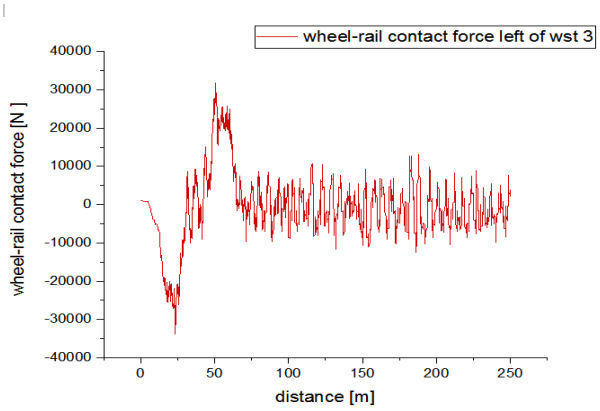

		Index	Value
wheel-rail contact force	Highest	628	26724.4
		627	26050.3
		641	25223.9
		626	24498.1
		629	24360.9
	Lowest	266	-21203.2
		267	-20725.1
		254	-20408
		262	-20350.8
		265	-20198.2

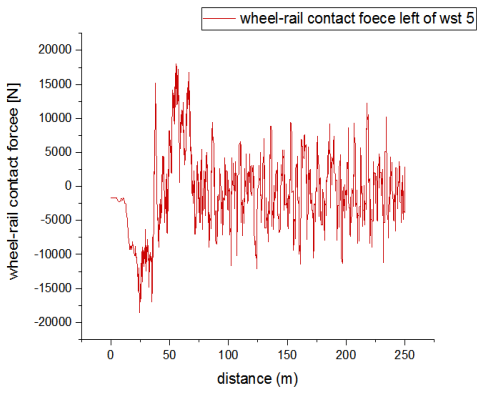

		Index	Value
wheel-rail contact force	Highest	666	18010.1
		674	17722.2
		673	17563
		686	17213.4
		665	17095.1
	Lowest	295	-18603.5
		296	-18367.2
		297	-17757.4
		298	-17310.3
		299	-17050.7

Figure 4-6 wheel-rail contact force left of wst1

From above table 4-5 the maximum value of wheel-rail contact force of wheel set 1 is 59.5% greater than that of wheel set 5. This indicates that there is no uniformity of load distribution to wheels which can be caused by non-uniformity of rail geometry in addition to vehicle motor position .so; left of of wheel set 1 wear earlier than the rest wheels.(refer appendix B).The normal force, wheel-rail contact force is a primary factor associated with wheel wear and is directly influenced to wheel loading conditions. The resulting wear index, wear rate, is a proportional function of the normal force, and is highly sensitive to the transverse or lateral profiles of the wheel and rail (contact geometry).

4.3 Wear index

Wear index from the following Figure is determined by SIMMPACK, 8.9 simulation model; the Models which assume the material loss is proportional to the frictional energy dissipated in the contact patch. Wear index is expressed as the sum of the products of the creepage and creep force, wear energy, in the lateral, longitudinal directions.. The degradation of wheels through wear and/or fatigue is often the primary driver behind the maintenance and replacement requirements for this critical component. The requirements and costs associated with these processes are closely linked to the operating conditions, which are a direct reflection of the track and rolling stock designs, the ongoing maintenance procedures and the way in which these are managed.

Due to higher impact occurrence at crossing it is very logical to be convinced that the stresses at crossing to be higher than the straight alignments. It is very visible on 2D results plotted in figure 4- .

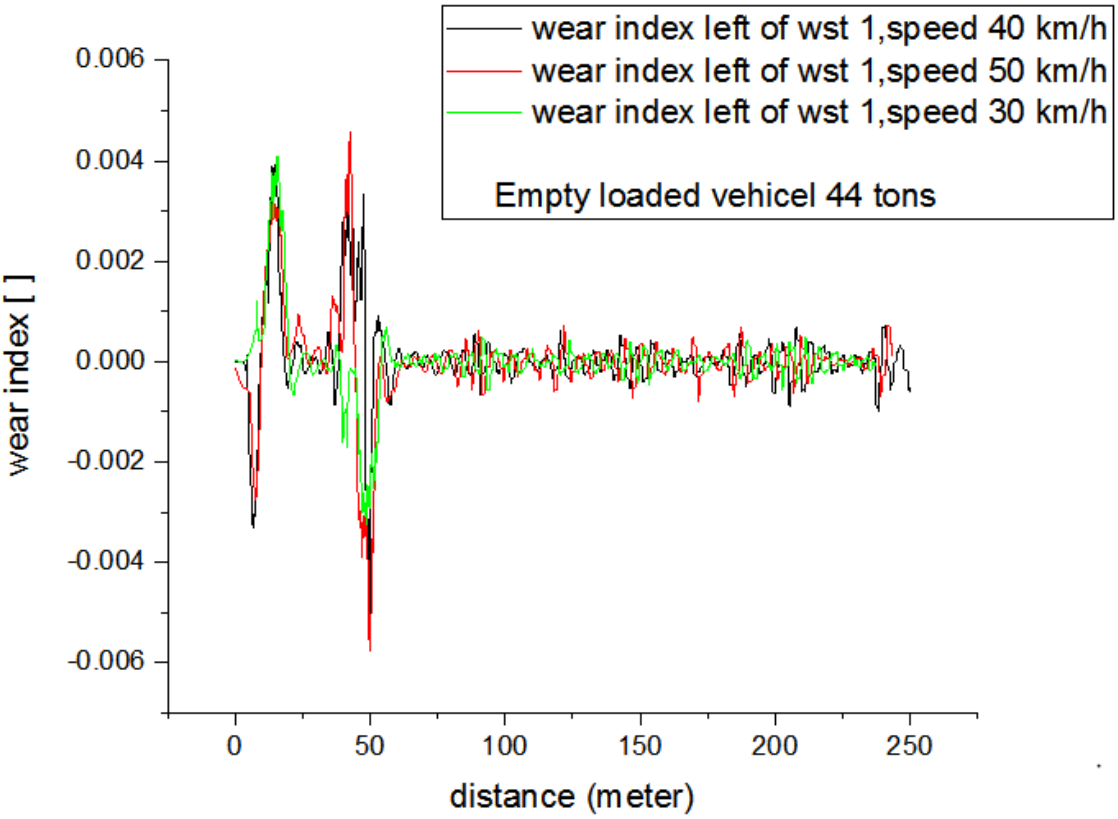

Figure 4-7 wear index – empty loaded vehicle

From figure 4-8 wear indexes is direct proportional to load and vehicle deriving speed. The Figure clearly shows the influence of train speed for empty loaded vehicle to be rather small. This observation is in accordance with the findings of the parametric study reported in [29]. We concluding that, the influence of train speed on contact pressure is small relative to fully loaded train. For the presented vehicle speed range of 30–50 km/h, it can be observed that the influence on wear energy development at the flange contact is limited

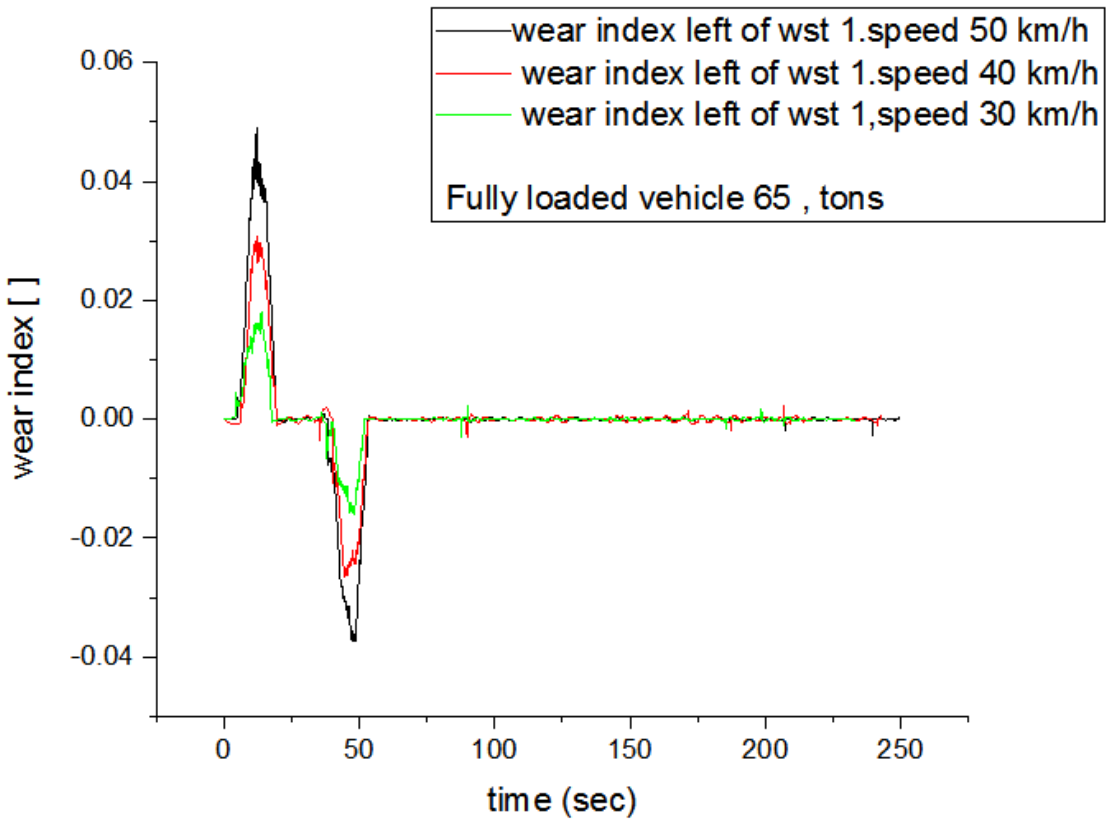

Figure 4-8 wear index- fully loaded vehicle

. Figure 4-8 presents the effect of train speed in relation to wear index of fully loaded vehicle, which is related with contact flange, Tγ, development at the leading wheel of the leading bogie. The result indicates that the wear index increases as driving speed increases. The effect is visible only at crossing. When negotiating the switch panel, distinct peaks for Tγ are seen to arise. These occur from changes in contact position and corresponding changes in locations and orientations of contact forces and slip. Upon entering the switch, a first peak for Tγ arises due to the appearing flange contact. A second peak occurs when the wheel load fully transfer from stock rail to switch rail.

From Table 4-4 the leading wheel set of the bogie has high amount of wear rate, the wear rate is maximum at wheel set 3.

4.4 Wear prediction

The Royal Institute of Technology Stockholm model is used to predict the wear rate. This model is based on an energy approach it uses wear coefficient as an input. This model is one of the most common models which have been used in recent works for wear modeling; accordingly, it has the same drawbacks as most of the classical wear models, which are dependent on the value of certain constants. The contact between wheel and rail is assumed to be an ellipse[4].

$$\text{Wear rate } (\mu g/m/mm^2) = \frac{ke * T * \gamma}{A} \qquad 4\text{-}5$$

Where, k_e is the wear coefficient in (µg/Nm), T is tractive force (N), v is total creepage between wheel and rail ,A is contact area in mm^2 , the waar condition through the total wheel sets are mild ,the wear coefficient $ke = 5.3$ [21]

Table 4-6 Wheel-rail tangential and global creepage force analyzed

Wheel set	**wst1**	**Wst2**	**wst3**	**Wst4**	**wst5**	**wst6**
Contact force, [N]	35300	26700	30300	31800	18000	28000
Global creepage ,γ, [N]	6582	6580	7990	7350	6910	7840
Contact area[mm^2]	52.86	45.4	49.2	50.81	34.77	46.61

4.4.1 Determining wheel-rail contact area

According to Hertz theory, the normal pressure in distributed as an ellipsoid over the elliptic contact area with semi-axis **a** and **b** the equation of ellipse

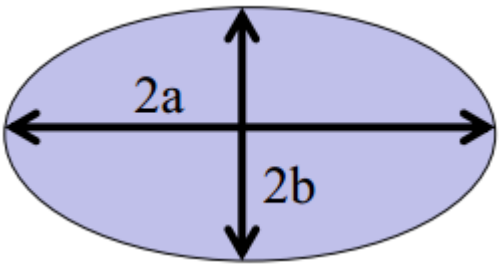

$$\frac{x^2}{a^2} + \frac{y^2}{b^2} = 1 \text{ Where } A = \frac{a}{b} \qquad 4\text{-}6$$

The ratio of the semi-axes A = a/b depends on the curvature of the wheel and the rail, and on the angle between the principal axes irrespective of the wheel load The contact area increases with the wheel load but the ratio a/b remains constant

Figure 4-17: area of ellipse

The semi-axes of the contact area, a and b, and the elastic deformation at the center

$$a = \left(\frac{3A^2E(1-\nu)}{2G\Sigma\frac{1}{r}}\right)^{\frac{1}{3}} * N^{1/3} \qquad b = \left(\frac{3E(1-\nu)}{2GA\Sigma\frac{1}{r}}\right)^{\frac{1}{3}} * N^{1/3} \qquad 4\text{-}7$$

Where: E is modulus of elasticity, G is the shear modulus and υ is Poisson's ratio the area of an ellipse is $A = \pi a \cdot b$ which wheel-rail contact in mm is.

Table 4-7 m and n as function of θ [17]

Θ (°)	m	n	Θ (°)	m	n	Θ (°)	m	n
0.5	61.400	0.1018	55.0	1.611	0.678	130.0	0.6410	1.754
1.0	36.890	0.1314	60.0	1.486	0.717	135.0	0.6040	1.926
1.5	27.480	0.1522	65.0	1.378	0.759	140.0	0.5670	2.136
2.0	22.260	0.1691	70.0	1.284	0.802	145.0	0.5300	2.397
3.0	16.500	0.1964	75.0	1.202	0.846	150.0	0.4930	2.731
4.0	13.310	0.2188	80.0	1.128	0.893	160.0	0.4123	3.813
6.0	9.790	0.2552	85.0	1.061	0.944	170.0	0.3112	6.604
8.0	7.860	0.2850	90.0	1.000	1.000	172.0	0.2850	7.860
10.0	6.604	0.3112	95.0	0.944	1.061	174.0	0.2552	9.790
20.0	3.813	0.4123	100.0	0.893	1.128	176.0	0.2188	13.310
30.0	2.731	0.4930	105.0	0.846	1.202	177.0	0.1964	16.500
35.0	2.397	0.5300	110.0	0.802	1.284	178.0	0.1691	22.260
40.0	2.136	0.5670	115.0	0.759	1.378	178.5	0.1522	27.480
45.0	1.926	0.6040	120.0	0.717	1.486	179.0	0.1314	36.890
50.0	1.754	0.6410	125.0	0.678	1.611	179.5	0.1018	61.400

Material propertiss

υ = 0.3 wheel radius r_{x1} =330 rail radius r_{y1} =300

E=210Gpa G = 81Gpa [10]

By using equation 4-5, 4- and 4-7 wear rate op each wheel set.

The above calculation was done according to the following formulas indicated below

Table 4-8 Wears cases regimes Styles [21]

Wear regime	**Wear range Tγ/A[N/ Tγ)**	**Wear rate µg/m/mm^2**
Mild	Tγ/A<10.4	5.3* Tγ/A
Serve	10.4 Tγ/A≤77.2	53.3
Catastrophic	Tγ/A≥77.3	60.9* Tγ/A

Table 4-9 Wear rate of more laded wheels

Wheel set (left)	**Wst 1**	**Wst 2**	**Wst 3**	**Wst 4**	**Wst 5**	**Wst 6**
Wear rate $(\frac{T\gamma}{A})$ µg/m/mm2	5.3*4.32=24.192	5.3*4.027 =21.3431	5.3*4.969 =26.3357	5.3*4.6 =24.38	5.3*3.57 =18.921	5.3*4.712 =16.973

According to (Joao Pombo, Jorge Ambrósio, Manuel Pereirathe) twin disc experimental data acquired from the contact between discs made of R8T wheel material and UIC50 900A rail material the wheel wear of all wheelsets are under mild regimes. According to the impute data the allowed material and design geometry is not the main case of excessive early weal wear

4.5 Mitigations of wheel wear.

Application of wheel and rail to lubricants containing extreme pressure (EP) additives, such as molybdenum disulphide (MoS2) or graphite, is by far the most effective approach to mitigating wheel wear and the one that can be implemented in LRT.

Altering wheel material by hard graded material is on option that can be considered to mitigate wheel wear. Mitigation by wheel-rail interface management is another mitigation method. This includes, examining regularly and limiting corrugation growth, vehicle stability and ride quality, friction management strategy, manage according to implementation and managing plan

CHAPTER 5 CONCLUSION AN RECOMMENDATION

This chapter is the final part of the study and gave a concluding remark of the work and then followed by propositions of some further works to be made that are recommended by the author for the better understanding and advancement of better knowledge in vehicle dynamics, track geometry on wear.

5.1 Conclusions

The study has performed the task of determining creepage and creep forces between wheel-rail contacts. It uses the wheel type s1002, and rail USC50 on crossing, by using MBS software. Varied speeds 30kmh, 40 and 50kmh are used, by considering empty and fully loaded vehicle under maximum load of 65 ton. The simulation was made and the results are used to determining wear index by using SIMPACKv8.9 MBS function.

Ward, Lewis and Dwyer-Joyce, wheel wear prediction tool, which uses wear coefficient based on energy approach is used to determine wear rate by using numerical method. The contact area between wheel and rail is assumed to be an ellipse.

The study investigate wheel wear regime by using Pombo, J., Ambrosio, J., Pereira, M., Lewis, R., Dwyer-Joyce, R., Ariaudo, C., & Kuka, formula. Wheel wear is not catastrophic, and it is under Mild wear regime, this indicates that crossing geometry and material properties allowed in design are not the major cases for excessive wheel wear of AALRT.

5.2 Recommendations

From analyzed result and discussions made the theoretical design parameters, material property specification is not the case for excessive wear of AALRT, so it is recommended to test the hardiness of material and compare it with the theoretical one.

Railway operating companies, rail track design engineers, rolling stock producing companies, are recommended to test material properties during design and before operation.

5.3 Future works

Even so some good achievements were obtained, but the work has been made with simplification and assumptions that made the study manageable in the time frame of the work and also with capable limitations. In order for maximizing the accuracy and precision of the research and gain an in depth understanding of the phenomenon, further works are in demand and includes the following but not limited to:

- ✓ Analyzing wear on curved section in detail and investigate whether the limited curve is the cause for excessive wear or not on study case,
- ✓ Investigating more experimental parameters, that influences vehicle dynamics in detail, and relate it with wear.
- ✓ Determine the material removal by using software and compare it with field measurement.

REFERENCES

[1] ADRIÁN SÁNCHEZ ARANDOJO. On validation of a wheel-rail, wear prediction code, Department of Aeronautical and Vehicle Engineering, Division of Rail Vehicles. Royal Institute of Technology Aeronautical and Vehicle Engineering Rail Vehicles SE-100 44 Stockholm

[2] Andersson, E berg M and Stichel S: rail vehicle dynamics Division of rail vehicle. Department of aeronautical and vehicle Engineering, Royal institute of Technology (KTH), stockholm 2007.

[3] ANDERSSON, MARTIN. "Derailment in track switches." Applied Mechanics, Chalmer University of Technology, Goteborg, 2012

[4] Andrian Sanichesz Arandojo, Validation of wheel-wail wear prediction code, department of aeronautical and vehicle Engineering, Royal institute of Thechnology (KTH),stockholm 2007.

[5] A.HUNT,GEOFFREY."Dynamic analysis of railway vehicle/track interaction forces." Loughborough University, 1986.

[6] Akchurin, Aydar; Bosman, Rob; Lugt, Piet M.; Drogen, Mark van (2016-06-16). "Analysis of Wear Particles Formed in Boundary-Lubricated Sliding Contacts". Tribology Letters.63 (2): 16. ISSN 1023-8883. doi:10.1007/s11249-016-0701-z.

[7] Beynon, J. H., Garnham, J. E., and Sawley, K. (1996).Rolling contact fatigue of three pearlitic rail steels. Wear, 192, 94-111.

[8] Bjorn, A. Palsson. "Optimization of Railway Switches and Crossing." Department of Applied Mechanics, CHALMERS UNIVERSITY OF TECHNOLOGY, Goteberg, 2014

[9]. Bevan, Adam, Molyneux Berry, Paul, Eickhoff, Bridget and Burstow, Mark (2013) Development and Validation of a Wheel Wear and Rolling Contact Fatigue Damage Model. Wear, 307 (12). Pp.100111. ISSN 00431648

[10]] China Railway Group Limited, Technical specification of vehicle, July, 2013

[11] Chattopadhyay, R. (2001). Surface Wear - Analysis, Treatment, and Prevention. OH, USA: ASM-International. ISBN 0-87170-702-0.

[12] D.Yu. Pogorelov, Simulation of rail vehicle dynamics with universal mechanism software //Rail vehicle dynamics and associated problems, Gliwice: Silesian University of Technology, 2005 – P.13-58

[13] Eric E. Mage, Rolling Contact Fatigue, 2011: A Comprehensive Review, Office of Railroad Policy and Development Washington, DC 20590

[14] Glaeser, W. A., *Prediction of Wheel/Rail Profile Wear*. Vehicle System dynamics Ed. (1993).

[15] Goreborg,Sweden, 2015,Kale Karttunen influence of wheel,rail and Truck geometry on wheel and rail degradation.

[16] I.Y. Shevtsov, V.L. Markine, C. Esveld, OPTIMAL DESIGN OF WHEEL PROFILE FOR RAILWAYVEHICLES, Faculty of Civil Engineering and Geosciences, Delft University of Technology CN Delft, P, 6 June, 2003

[17] J. Piotrowski, W. Kik, A simplified model of wheel/rail contact mechanics for non-Hertzian problems and its application in rail vehicle dynamic simulations // Vehicle System Dynamics. – 2008. – Vol.46(1-2). – P.27-48

[18] J. Santamaria*, E.G. Vadillo, O. Oyarzabal, Wheel-rail wear index prediction considering multiple contact patches, Department of Mechanical Engineering. University of the Basque Country. Alda. Urquiso s/n 48013 Bilbao, Spain

[19] J. Kalker, Three-Dimensional Elastic Bodies in Rolling Contact, Kluwer Academis Publishers, Dordrecht, 1990.

[20] Katsuya Tanifuji Niigata,A Study on Prediction of Wear Progress of Railway Wheel, University Japan, Stevinweg 1, NL-2628,

[21] Pombo, J., Ambrosio, J., Pereira, M., Lewis, R., Dwyer-Joyce, R., Ariaudo, C., & Kuka, N. (2010). A Railway Wheel Wear Prediction Tool based on a Multi-body Software Journal of Theoretical and Applied Mechanics, 48(3), 751-770.

[22] Rabinowicz, E. (1995).Friction and Wear of Materials.New York,John Wiley and sons.

[23] Roger Enblom, Simulation of Railway Wheel Profile Evolution due to Wear, Vehicle Dynamics team Specialist Engineering department Mainline and Metros division Västerås, Sweden

[24]. SIMPACK Reference Guide SIMPACK Release 8.9, September 1, 2010/SIMDOC v8.904

[25]. T, Jendel, M. Berg, Prediction of wheel profile wear, Vehicle System Dynamics Supplement, Vol. 37, pp. 502-513, 2002

[26] Williams, J. A. (2005). "Wear and wear particles - Some fundamentals." Tribology International 38(10): 863-870

[27] https://en.mWikipedia,org

[28] Ward A, Lewis R and Dwyer-Joyce R S: Incorporating a railway wheel wear model Into multi-body simulations of wheelset dynamics, Tribology Series 41:367-376, Department of Mechanical Engineering, University of She-eld, She-eld 2002

[29] Kassa E, Johansson G. Simulation of train-turnout interaction and plastic deformation of rail profles. Veh Syst Dyn. 2006;44:349–359

APPENDEX A

Some 2D simulation results

Longitudinal and Lateral Creepage on wheels of leading wheel sets

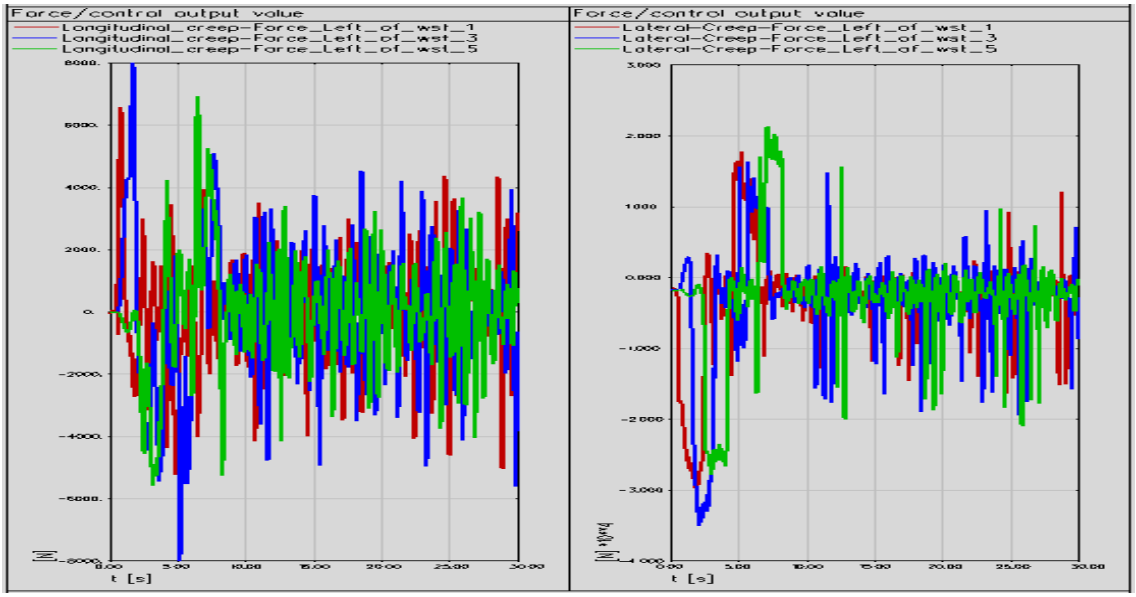

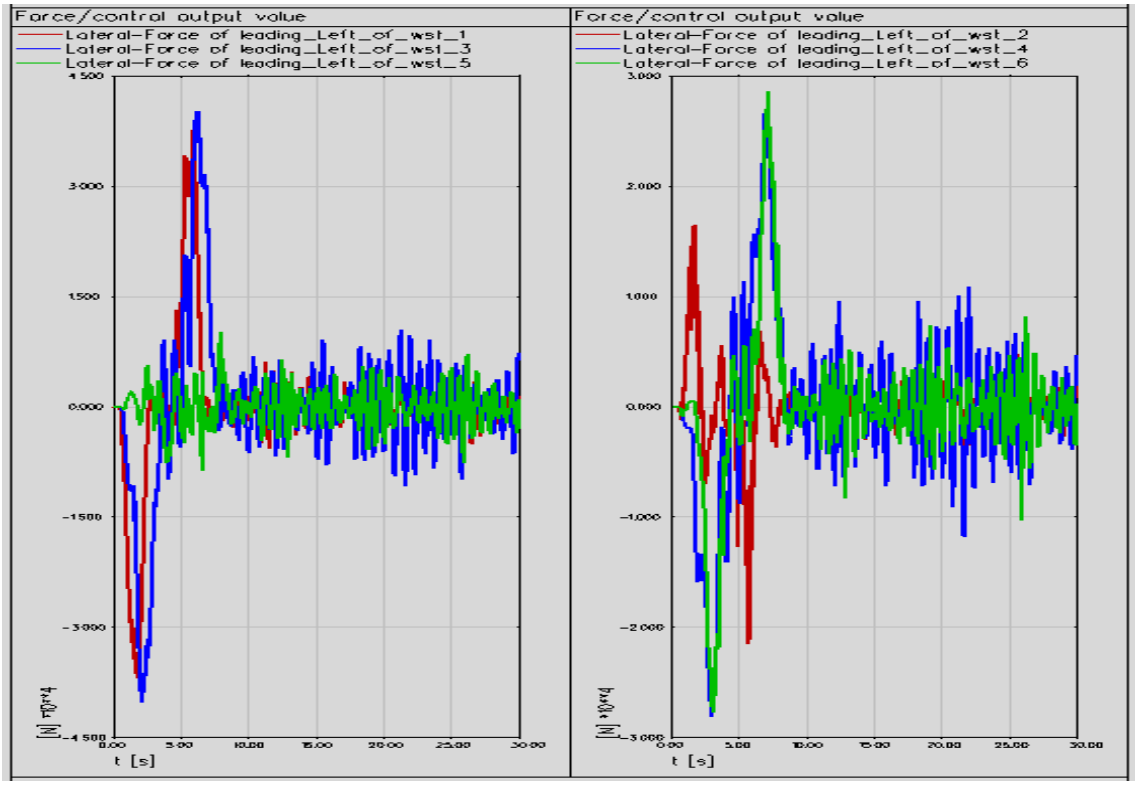

Lateral Force of each wheels of loading Wheel sets

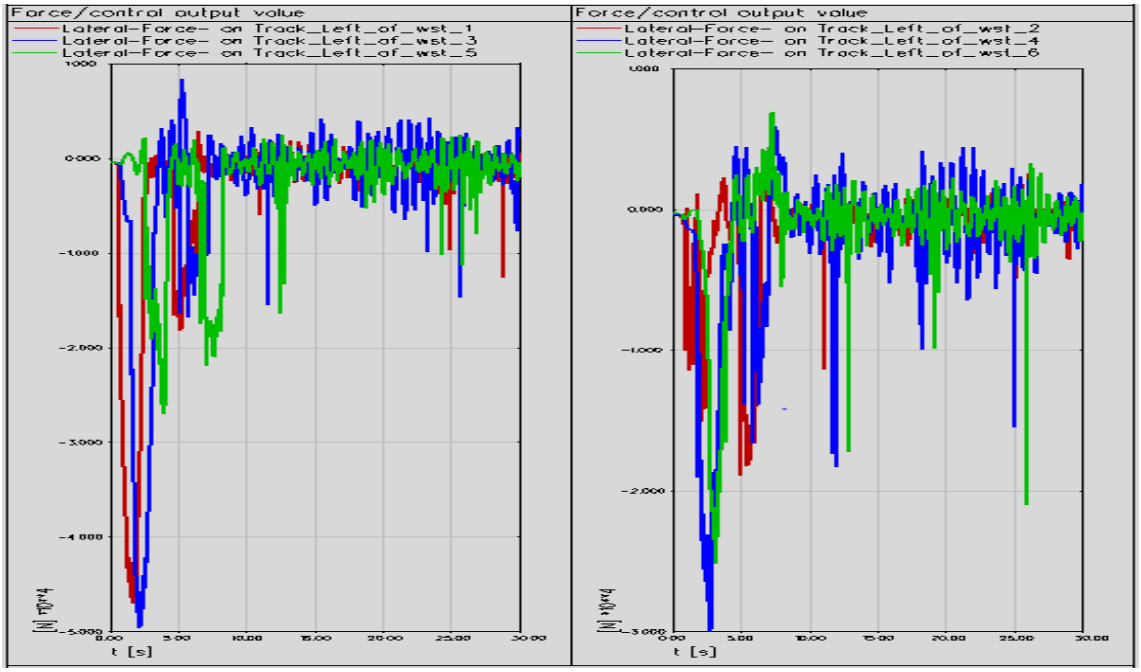

Lateral Force of Wheel set on Track

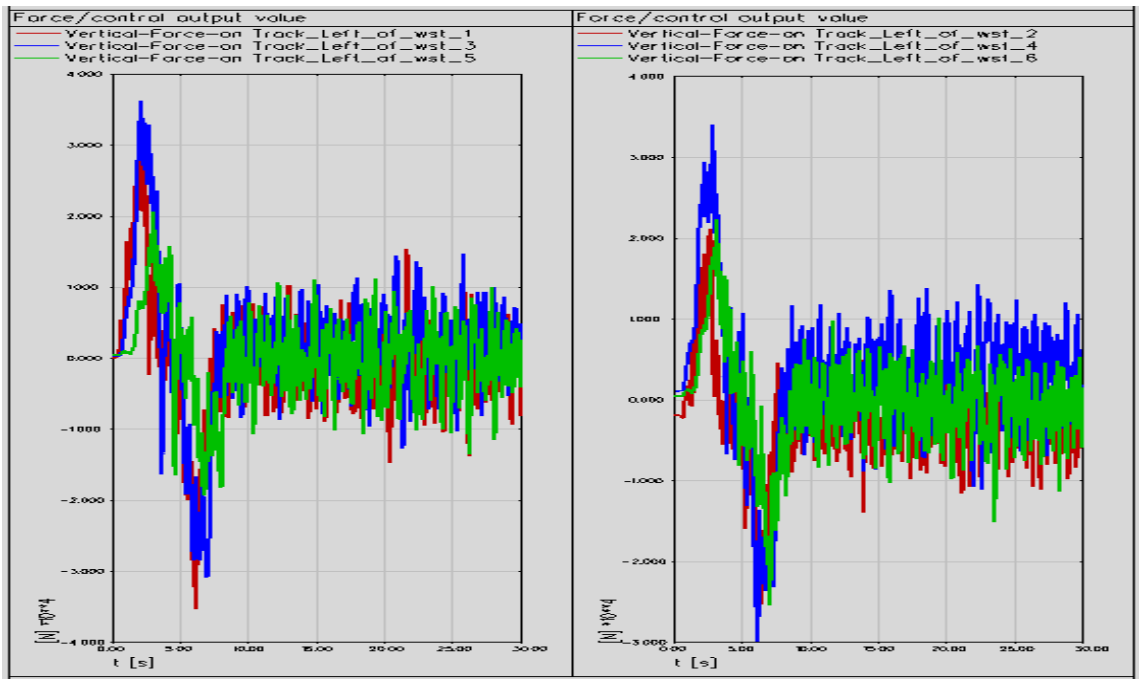

Vertical Force of each wheel set on Track

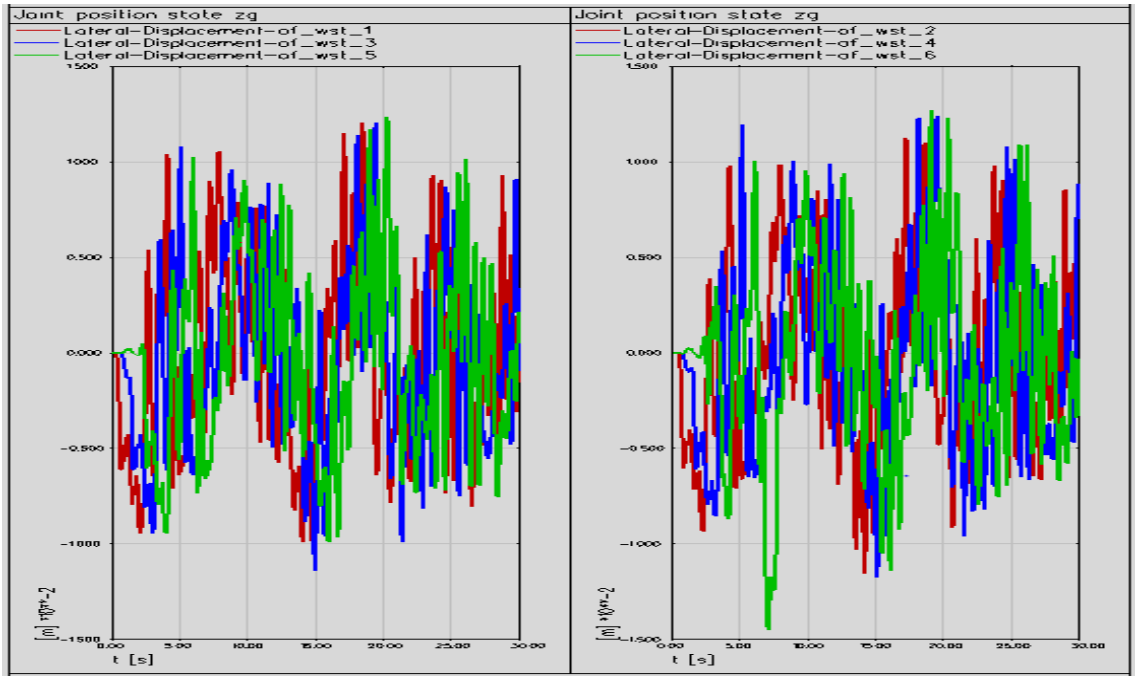

Lateral Displacement of each Wheel set

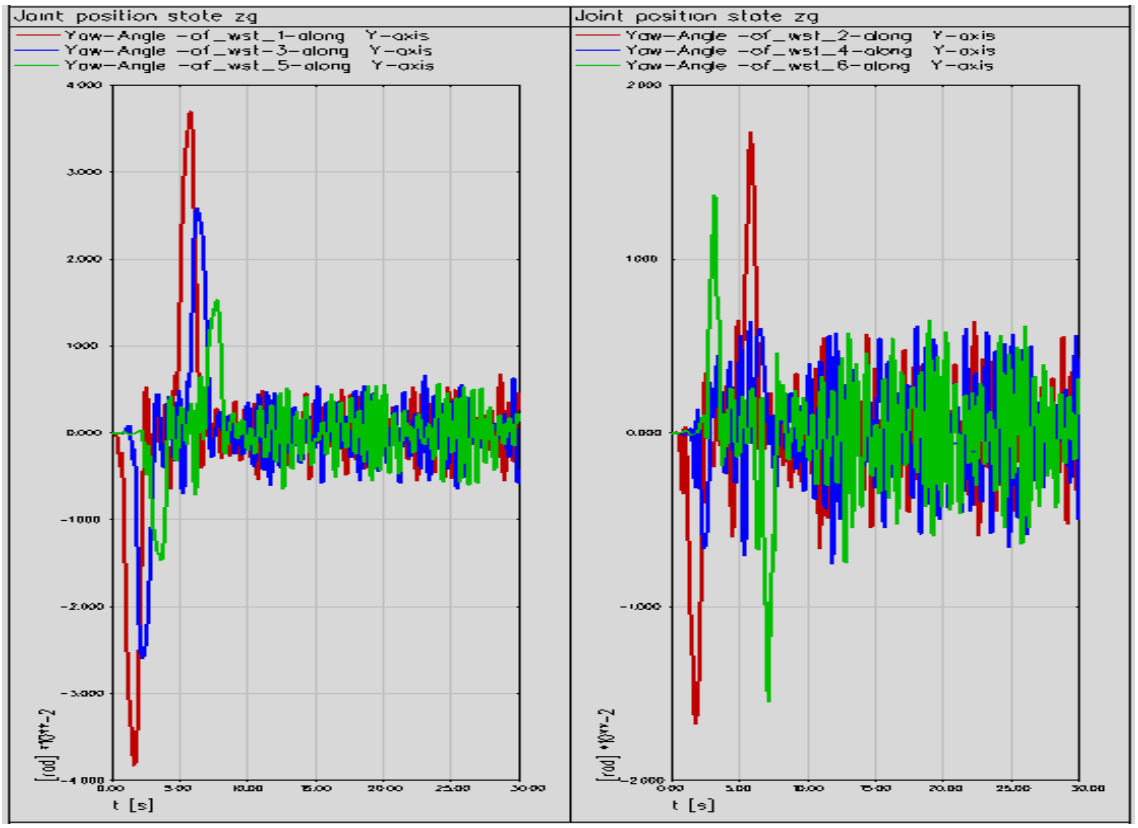

Yaw-Angle of each Wheel set along X-axis

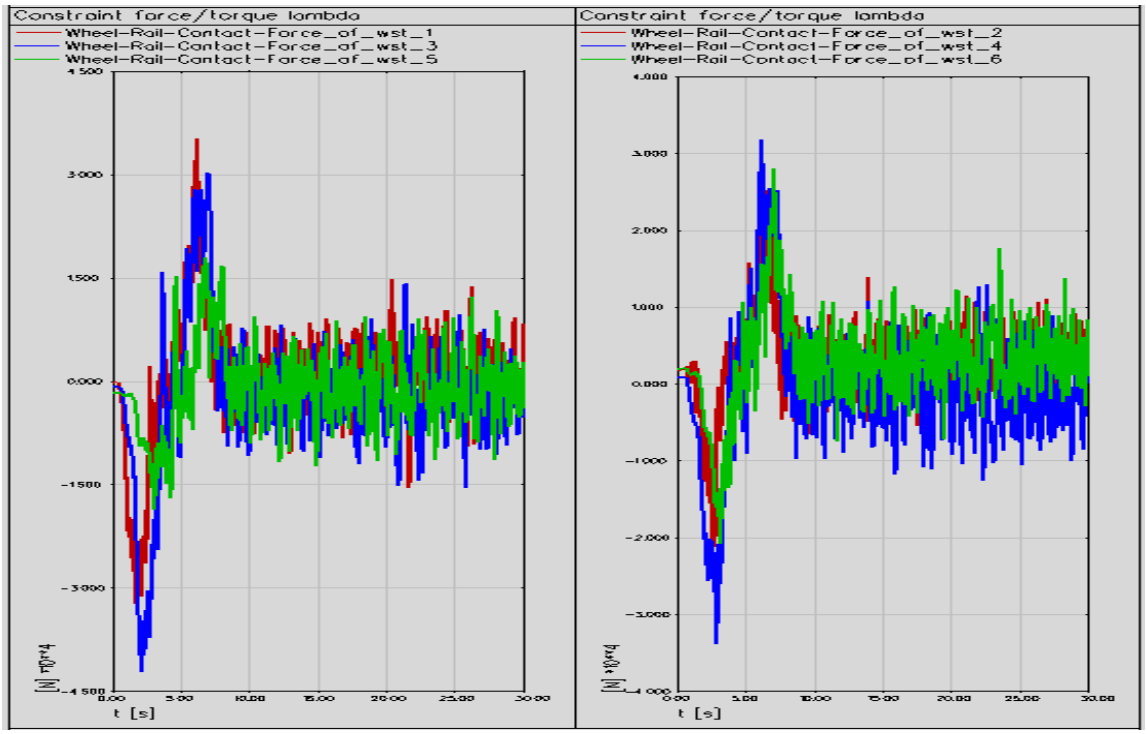

Wheel-Rail Contact Force of each wheel set

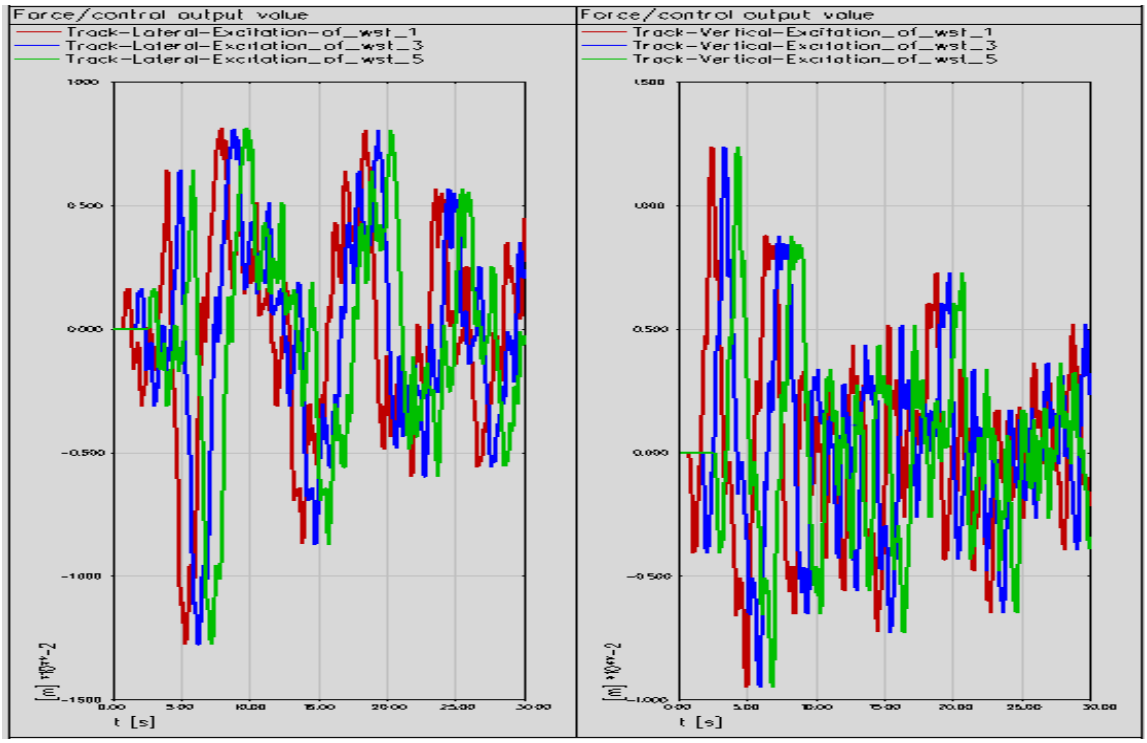

Track Lateral and Vertical Excitation of Leading wheel set

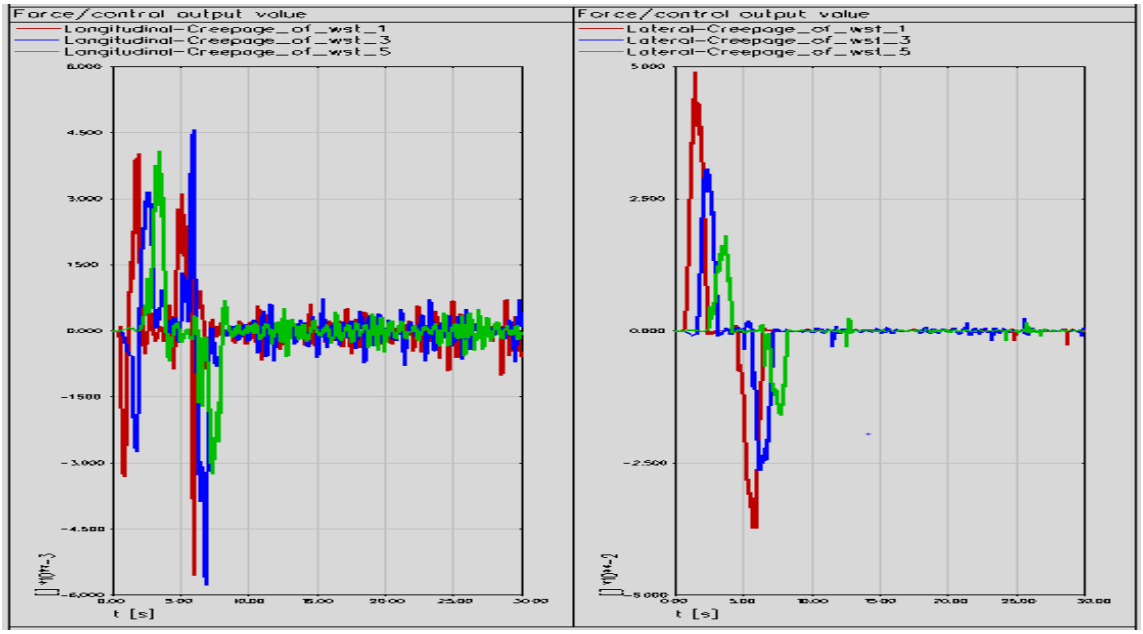

figure.. Longitudinal and Lateral creepage on leading wheel set

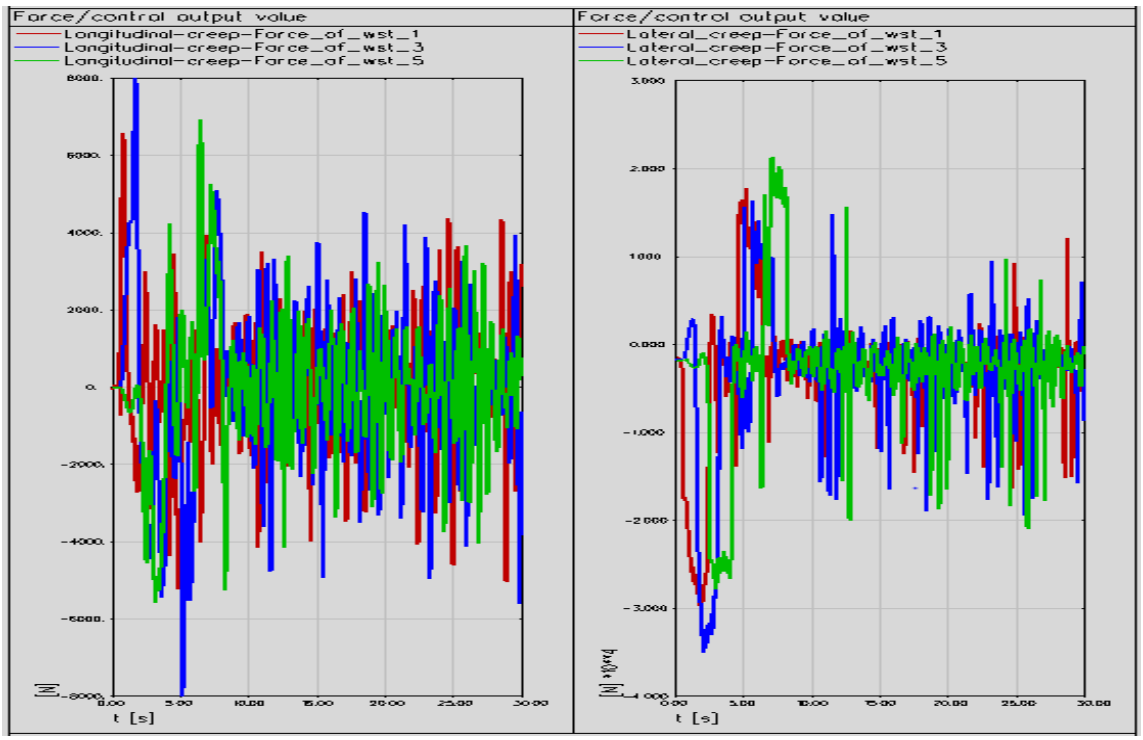

Longitudinal and Lateral creep Force on Leading wheel set

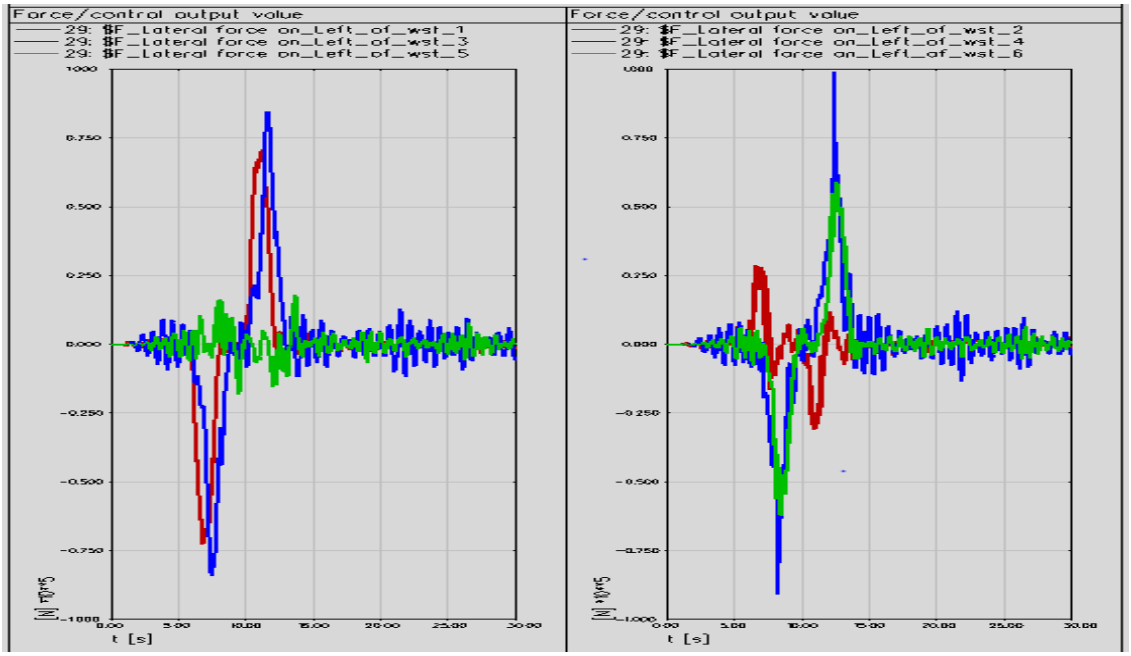

Figure. Lateral Force of each wheel set

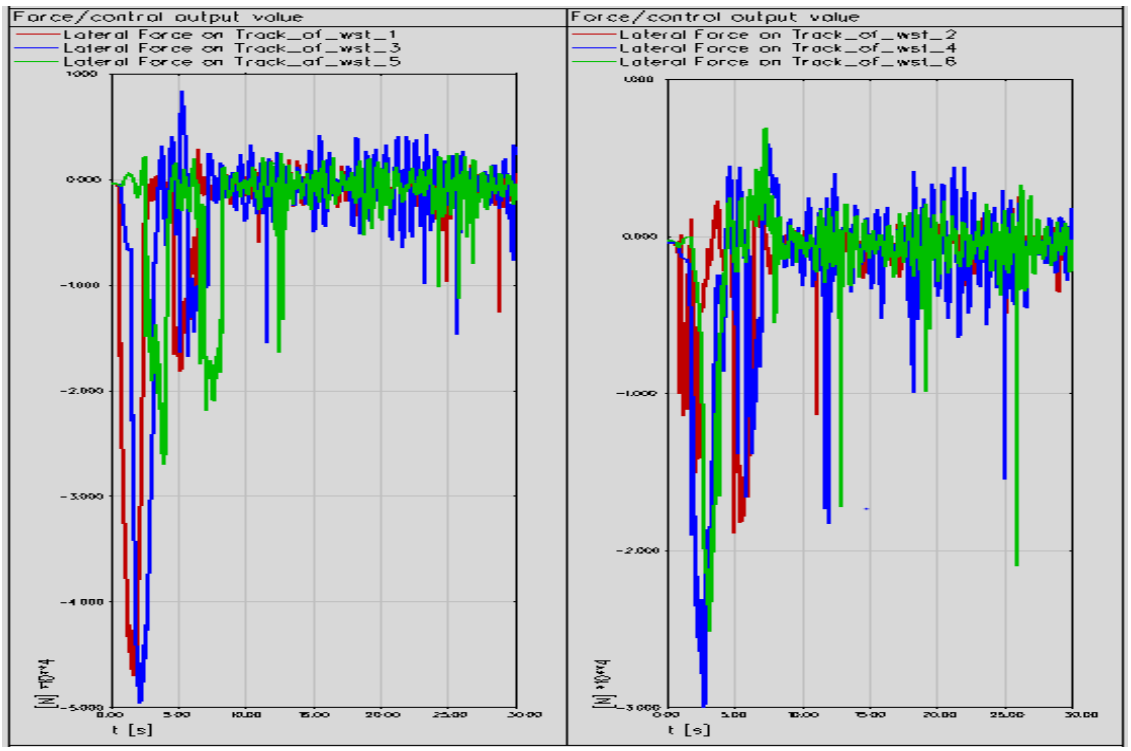

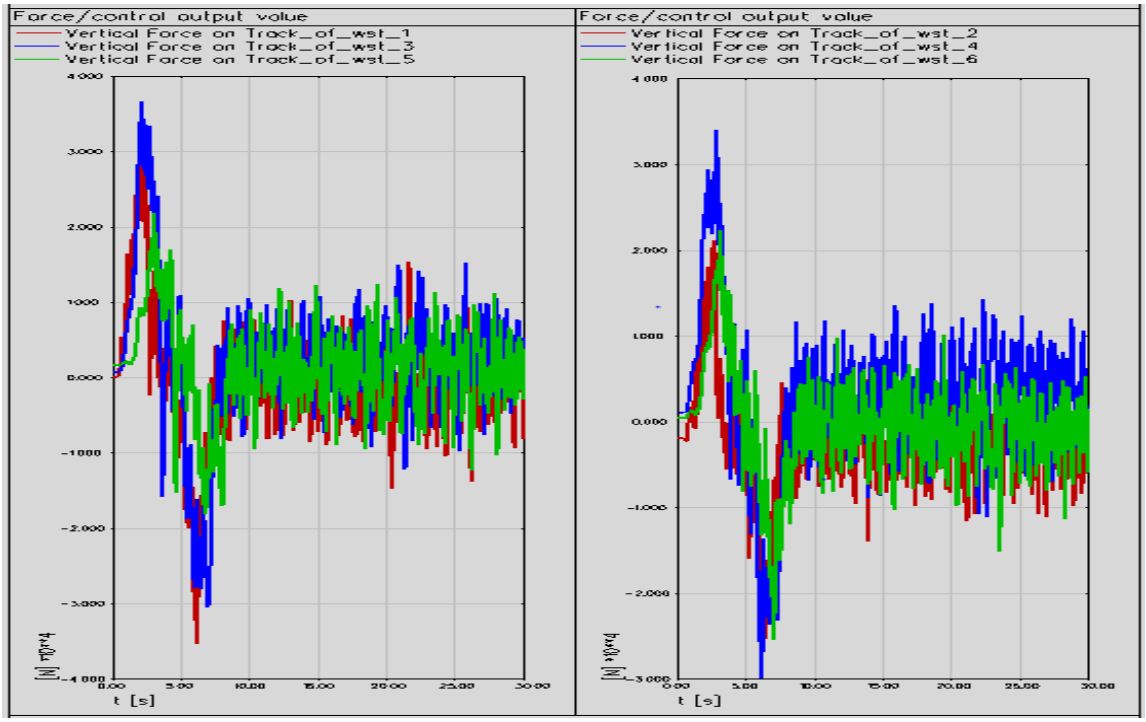

figure ... vertical Force on Track of each wheel set

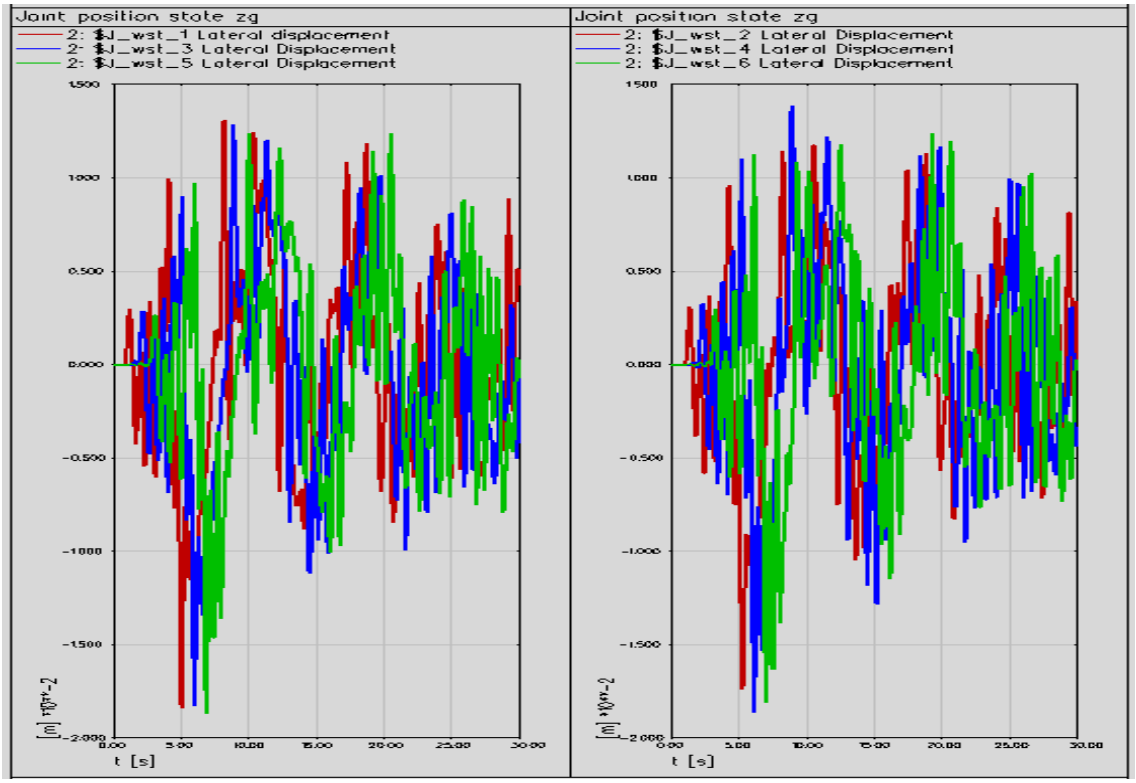

Figure.. Lateral Displacement of each wheel set

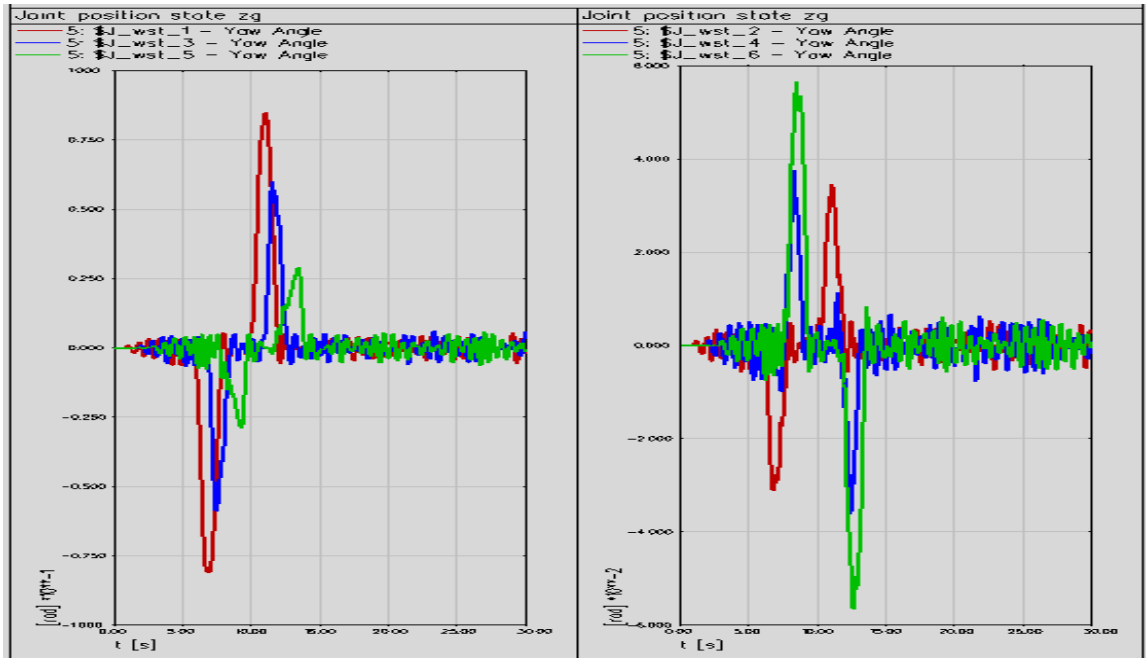

Figue.... Yaw Angle of each wheel set along y-axis

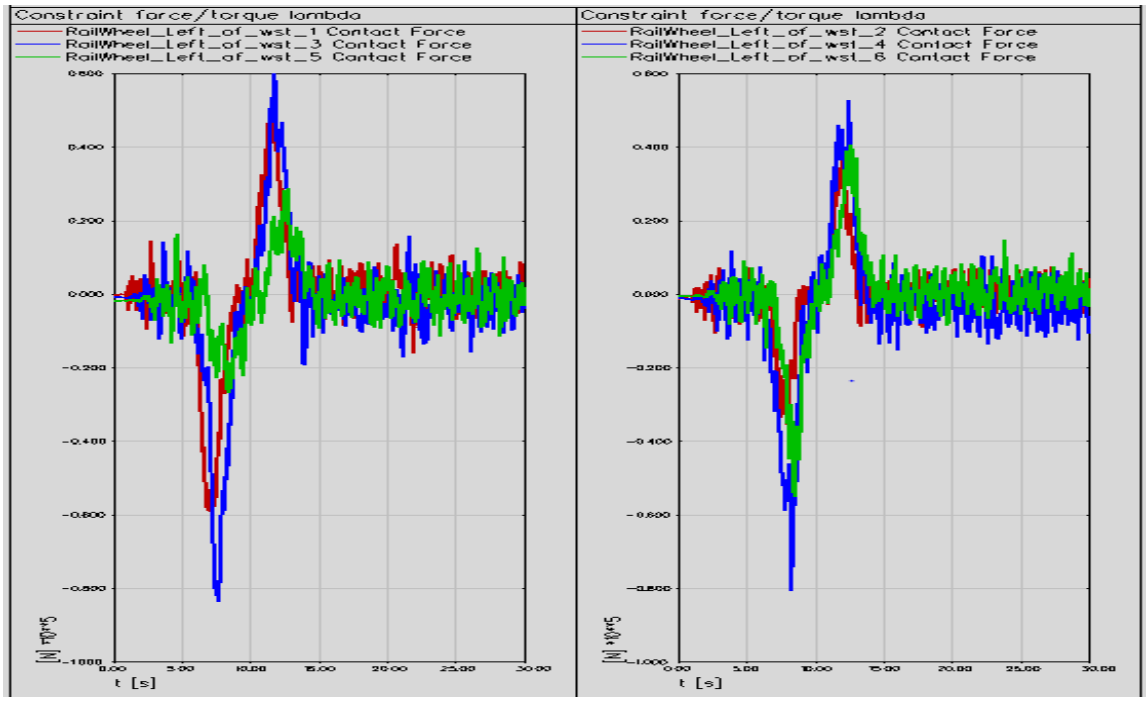

Wheel- Rail contact Force of each wheel set

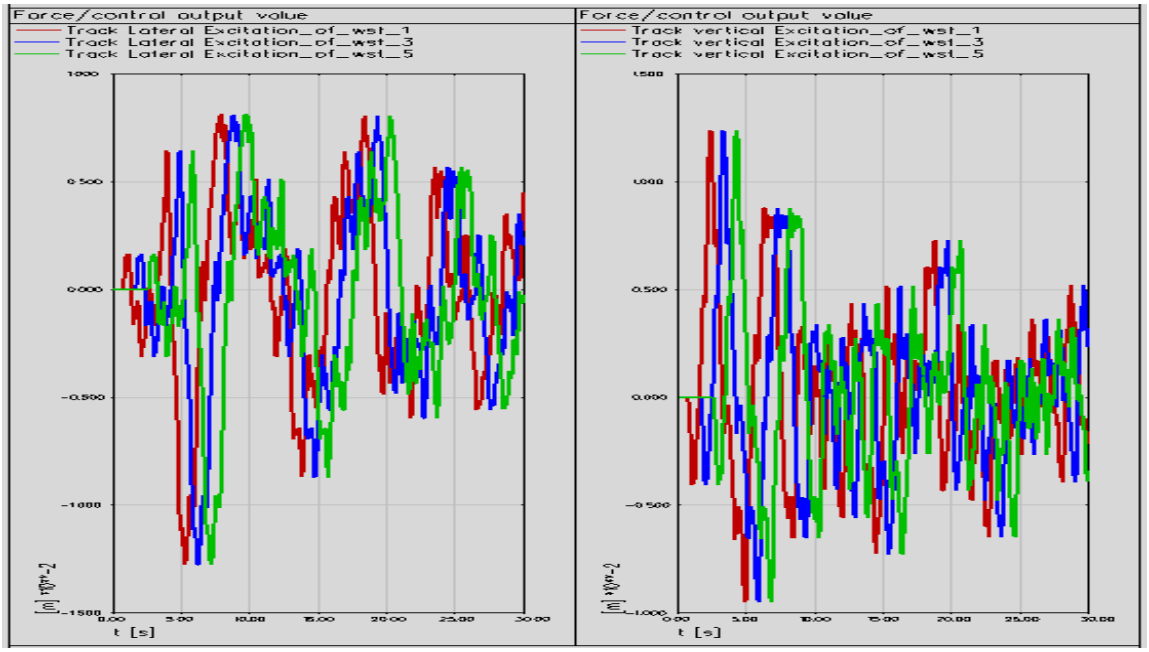
Force/control output value
Track Lateral Excitation_of_wst_1
Track Lateral Excitation_of_wst_3
Track Lateral Excitation_of_wst_5
t [s]
Force/control output value
Track vertical Excitation_of_wst_1
Track vertical Excitation_of_wst_3
Track vertical Excitation_of_wst_5
t [s]

APPENDEX B

No.	Date	meal age	vehicle No.	wheelset No.	pre-measurement					post-measurement						remark
					diameter difference	diameter		flange thickness		diameter difference	diameter		flange thickness		total re-profiled wheelset	
						left	right	left	right		left	right	left	right		
1	3-9/2/2016	4888	104	1	0.08	660.66	660.58	23.25	23.26	-	-	-	-	-		burn on wheel thread
				2	0.1	660.54	660.64	23.18	23.3	-	-	-	-	-		
				3	0.67	659.87	660.55	22.4	22.97	1.77	**650.17**	**651.94**	19.75	19.96	1	
				4	0.21	660.45	660.66	22.95	22.51	0.06	**652.53**	**652.59**	20.6	21.03	2	
				5	0.15	660.48	660.63	23.07	23.19	-	-	-	-	-		
				6	0.06	660.47	660.53	23.53	23.36	-	-	-	-	-		
2	15-18/03/2016	6065	104	1	0.14	660.63	660.49	23.27	23.13	-	-	-	-	-		burn on wheel threa
				2	0.04	660.51	660.55	22.95	23.25	-	-	-	-	-		

				3	0.76	651.06	651.82	19.62	19.74	1.36	**649.92**	**651.28**	19.58	19.75	3	d
				4	0.01	652.48	652.46	20.27	20.79	0.16	**651.36**	**651.2**	20.21	20.05	4	
				5	0.13	660.46	660.6	23.19	23.34	-	-	-	-	-		
				6	0.22	660.51	660.29	23.4	23.15	-	-	-	-	-		
3	25/03/2016 to 11/04/2016	30478	119	1	0.1	660	659.9	20.24	21	-	-	-	-	-		scratch on wheel thread
				2	0.15	659.94	660.1	20.82	20.81	-	-	-	-	-		
				3	0.01	660.36	660.37	19.77	20.4	0.3	**655.15**	**655.45**	22.28	22.3	5	
				4	0.49	660.79	660.29	20.18	19.45	0.39	**656.82**	**656.43**	19.65	19.71	6	
				5	0.08	660.13	660.05	20.75	20.62	-	-	-	-	-		
				6	0.09	660.13	660.03	21.08	20.83	-	-	-	-	-		
4	7-8/5/2016	no	213	1	0.53	659.07	659.6	16.74	17.04	0.01	**639.73**	**639.73**	19.88	19.86	7	wheel flange thickness
				2	0.84	659.34	658.5	17.5	14.61	0.16	**635.17**	**635.01**	19.41	19.57	8	
				3	-	-	-	-	-	-	-	-	-	-		
				4	-	-	-	-	-	-	-	-	-	-		
				5	0.1	659.69	659.79	15.7	17.56	-	-	-	-	-		

				6	0.35	659.54	659.19	17.77	15.49	-	-	-	-	-		
5	8-10/6/2016	26848	211	1	0.14	659.87	660.01	19.11	19.42	-	-	-	-	-		wheel flange thickness
				2	0.32	659.97	659.65	17.89	18.32	-	-	-	-	-		
				3	0.61	651.4	652.01	19.09	18.98	0.01	**640**	**639.99**	18.87	18.31	9	
				4	0.71	660.83	660.12	19.09	13.24	0.35	**634.84**	**635.18**	19.52	18.74	10	
				5	0.21	659.93	660.14	19.19	19.35	-	-	-	-	-		
				6	0.11	659.91	660.03	19.46	17.03	-	-	-	-	-		
6	11-12/6/2016	56447	209	1	0.2	659.18	659.38	15.34	17.24	0.41	**650.82**	**651.23**	17.3	17.3	11	scratch on wheel thread
				2	0.09	659.42	659.33	15.97	15.58	0.04	**650.91**	**650.95**	17.62	17.69	12	
				3	0.16	660.16	660	17.21	17.5	0.11	**648.69**	**648.58**	20.02	20.03		
				4	0.08	659.8	659.88	15.28	16.31	0.14	**648.47**	**648.61**	19.08	18.99		
				5	0.23	659.36	659.59	17.34	17.27	-	-	-	-	-		
				6	0.02	659.28	659.3	16.43	15.18	0.22	**654.08**	**654.3**	17.01	16.85	13	
7	12-	3595	216	1	0.18	659.	659.79	16.81	17.78	0.4	**649.8**	**650.2**	19.1	19.	14	wheel

	14/06/2016	5				61					**2**	**3**	7	16		flange thickness
				2	0.07	659.74	659.8	15.25	14.45	0.12	**646.73**	**646.61**	17.94	17.87		
				3	0	660.32	660.32	18.13	17.95	-	-	-	-	-		
				4	0.07	660.35	660.29	18.5	18.46	-	-	-	-	-		
				5	0.23	659.78	660.01	17.49	16.6	0.17	**648.19**	**648.37**	20.21	19.9	15	
				6	0.02	659.76	659.74	18.28	14.84	0.6	**648.18**	**648.78**	18.58	18.35	16	
8	14-16/6/2016	44026	212	1	0.04	659.66	659.63	16.06	17.5	0.03	**641.17**	**641.14**	19.86	19.7	17	
				2	0.33	659.73	659.4	17.02	13.66	0.07	**638.31**	**638.38**	18.41	18.4	18	
				3	0.01	660.12	660.13	16.49	17.69	0.38	**653.41**	**653.03**	18.42	18.6	19	
				4	0.12	660.09	660.21	17.48	17.62	0.26	**653.65**	**653.39**	19.51	19.53	20	
				5	0.54	659.34	659.88	16.63	19.38	0.05	**653.52**	**653.58**	18.36	18.36	21	
				6	0.06	659.55	659.49	16.41	16.93	0	**653.14**	**653.15**	18.14	18.07	22	
9	17-18/6/2016	6518	107	1	0.25	659.56	659.32	19.92	20.31	-	-	-	-	-		wheel flange thick
				2	0.04	659.46	659.51	19.75	19.65	-	-	-	-	-		

				3	0.3	660.1	660.39	18.2	16.09	0.31	**649.78**	**650.09**	18.68	18.87	23	ness
				4	0.32	660.09	660.41	17.95	14.81	0.32	**650.08**	**650.13**	18.03	17.86	24	
				5	0.36	659.73	659.37	19.28	19.51	-	-	-	-	-		
				6	0.07	659.51	659.44	20.08	20.31	-	-	-	-	-		
10	18-21/06/2016	35568	217	1	0.13	656.07	656.19	16.65	17.01	0.16	**652.04**	**652.2**	17.13	17.61	25	
				2	0.06	659.73	659.67	17.61	16.83	0.31	**655.46**	**655.77**	18.27	18.22	26	
				3	0.19	651.07	650.87	18.04	18.45	0.06	**641.08**	**641.14**	19.55	19.86	27	
				4	0.11	645.06	644.95	16.66	16.82	0.05	**640.98**	**641.03**	17.02	17.15	28	
				5	0.21	659.73	659.94	18.32	18.89	-	-	-	-	-		
				6	0.05	659.65	659.7	17.52	16.36	-	-	-	-	-		
11	4-24/06/2016	53109	206	1	0.39	659.05	659.44	16.25	17.22	0.16	**649.24**	**649.4**	18.97	19.38	29	wheel flange thickness
				2	0.06	659.3	659.24	16.87	15.14	0.16	**648.08**	**648.21**	18.04	18.57	30	
				3	0.29	660.31	660.02	14.01	15.07	0.16	**639.04**	**639.31**	18.56	18.8	31	
				4	0.23	660.	659.98	12.45	14.48	0.16	**637.6**	**637.9**	17.6	17.	32	

						21					**3**	**6**	8	94		
				5	0.21	659.35	659.55	17.35	16.63	0.16	**653.16**	**653.6**	17.9	18.01	33	
				6	0.02	659.44	659.46	15.92	15.36	0.16	**653.2**	**653.42**	17.61	17.91	34	
12	24-26/06/2016	45540	115	1	0.17	659.66	659.49	20.62	19.75	-	-	-	-	-		wheel flange thickness
				2	0.18	659.83	659.65	20.39	20.28	-	-	-	-	-		
				3	0.41	659.89	660.3	19.2	15.13	0.92	**635.37**	**636.3**	20	20.79	35	
				4	0.32	659.94	660.26	19.77	14.08	0.37	**635.29**	**635.66**	19.25	19.38	36	
				5	0.22	659.87	659.65	20.71	20.59	-	-	-	-	-		
				6	0.18	659.6	659.41	20.45	19.91	-	-	-	-	-		
13	27/6-1/7/2016	49030	205	1	0.11	659.42	659.53	16.71	16.54	0.44	**639.66**	**640.09**	20.31	20.09	37	wheel flange thickness
				2	0.02	659.62	659.64	17.48	13.48	0.47	**637.17**	**637.64**	17.56	17.56	38	
				3	0.04	660.15	660.19	17.38	18.24	-	-	-	-	-		
				4	0.08	659.96	660.04	16.38	17.37	-	-	-	-	-		
				5	0.04	659.55	659.59	16.48	16.59	-	-	-	-	-		

				6	0.08	659.61	659.69	17.59	18.51	-	-	-	-	-		
14	3-7/7/2016	54471	218	1	0.3	659.29	659.59	13.7	16.65	0.24	**642.86**	**643.11**	17.65	17.59	39	wheel flange thickness
				2	0.15	659.29	659.44	14.16	13.86	0.32	**643.27**	**642.96**	17.58	17.67	40	
				3	0.01	660.19	660.21	17.08	16.14	0.24	**636.55**	**636.79**	19.55	19.72	41	
				4	0.16	660.08	659.92	14.11	12.83	0.32	**637.96**	**638.28**	17.69	17.78	42	
				5	0.53	659.12	659.65	18.38	18.06	0.03	**647.98**	**647.95**	21.11	20.85	43	
				6	0.41	658.94	659.34	16.02	15.26	0.22	**648.16**	**647.94**	17.83	17.78	44	
15	08-11/07/2016	47312	215	1	0.44	659.56	660	17.07	17.93	0.31	**640.76**	**641.07**	20.97	21.08	45	wheel flange thickness
				2	0.06	659.79	659.73	15.46	13.46	0.1	**642.02**	**642.12**	17.44	17.55	46	
				3	0.09	660.33	660.41	18.05	16.75	0.3	**645.14**	**645.44**	19.71	19.94	47	
				4	0.18	660.1	660.28	17.09	15.45	0.21	**644.17**	**644.38**	18.82	18.81	48	
				5	0.02	659.79	659.81	16.54	16.65	-	-	-	-	-		
				6	0.17	659.79	659.62	16.17	16.03	-	-	-	-	-		
16	13-	2228	207	1	0.19	659.	660.15	18.63	20.02	0.1	**655.1**	**655.2**	19.5	19.	49	

	14/07/2016	2				96					**7**	**7**	9	84		
				2	0.08	660	659.92	18.48	17.54	0.1	**654.87**	**654.76**	18.91	18.96	50	
				3	0.01	660.32	660.33	19.54	19.36	-	-	-	-	-		
				4	0.06	660.26	660.32	18.13	18.11	-	-	-	-	-		
				5	0.12	659.98	660.1	19.37	18.82	-	-	-	-	-		
				6	0.06	659.94	660	19.06	17.62	-	-	-	-	-		
17	15-27/07/2016	43452	208	1	0.07	659.43	659.5	16.34	17.53	0.29	**637.93**	**638.21**	20.11	20.24	51	wheel flange thickness
				2	0.22	659.56	659.78	13.45	18.34	0.19	**635.4**	**635.21**	17.41	17.75	52	
				3	0.15	660.14	660.29	17.05	15.44	0.1	**640.15**	**640.05**	18.58	18.78	53	
				4	0.06	660.19	660.12	17.28	14.47	0.23	**639.02**	**638.79**	18.3	18.3	54	
				5	0.12	659.67	659.56	18.68	16.96	0.19	**645.95**	**645.76**	19.68	19.82	55	
				6	0.2	659.36	659.55	17.09	15.99	0.07	**645.78**	**645.86**	18.86	18.9	56	
18	17-18/08/2016	45551	114	1	0.12	659.86	659.74	19.6	20.48	-	-	-	-	-		
				2	0.1	659.85	659.95	20.29	20.47	-	-	-	-	-		

				3	0.25	660.3	660.05	18.52	19.71	0.35	**655.78**	**655.43**	18.67	19.38	57	
				4	0.25	660.27	660.02	18.4	19.63	0.58	**655.16**	**655.75**	19.35	19.26	58	
				5	0.09	659.88	659.79	19.68	20.34	-	-	-	-	-		
				6	0.12	659.79	659.67	21.11	19.99	-	-	-	-	-		
19	9-22/08/2016	51662	210	1	0.32	659.02	659.34	16.12	16.36	0.29	**642.73**	**642.44**	18.99	18.99	59	wheel flange thickness
				2	0.24	659.44	659.2	16.3	14.39	0.61	**642.23**	**641.63**	17.75	18.09	60	
				3	0.23	660.06	660.3	15.52	14.21	0.39	**640.74**	**641.13**	17.39	17.46	61	
				4	0.21	650.68	650.89	17.51	17.45	0.05	**642.57**	**642.52**	18.1	18.44	62	
				5	0.2	659.25	659.45	16.4	16.93	0.15	**646.23**	**646.37**	18.02	18.11	63	
				6	0	659.15	659.16	16.38	14.98	0.41	**645.96**	**645.55**	17.27	17.58	64	
20	23-25/08/2016	40415	108	1	0.42	659.94	659.52	20.44	20.4	-	-	-	-	-		
				2	0.03	659.67	659.64	19.94	19.66	-	-	-	-	-		
				3	0.21	660.49	660.28	18.59	17.81	0.65	**654.65**	**655.3**	18.52	18.82	65	
				4	0.13	660.	660.28	17.9	16.94	0.23	**654.0**	**654.5**	18.5	18.	66	

						15					**1**	**4**	4	87		
				5	0.38	659.94	659.56	19.64	19.67	-	-	-	-	-		
				6	0.37	659.9	659.53	20.05	20.08	-	-	-	-	-		
21	25-30/08/2016	45551	111	1	0.44	659.16	658.73	18.52	18.79	-	-	-	-	-		wheel flange thickness
				2	0.19	**658.93**	**658.74**	18.05	18.59	-	-	-	-	-		
				3	0.53	659.83	660.36	17.14	13.11	0.31	**636.12**	**636.43**	17.94	17.76	67	
				4	0.56	659.73	660.29	17.26	13.04	0.51	**635.31**	**635.82**	17.23	16.99	68	
				5	0.09	659.88	659.79	19.68	20.34	-	-	-	-	-		
				6	0.12	659.79	659.67	21.11	19.99	-	-	-	-	-		
22	05-07/09/2016	54807	110	1	0.22	659.34	659.12	18.71	19.11	-	-	-	-	-		wheel flange thickness
				2	0.23	659.41	659.18	18.86	18.64	-	-	-	-	-		
				3	0.31	659.99	660.31	17.13	14.58	1.1	**637.47**	**636.36**	18.33	18.75	69	
				4	0.58	659.8	660.37	17.02	13.09	0.22	**636.5**	**636.28**	18.24	18.07	70	
				5	0.5	659.79	659.29	19.71	18.67	-	-	-	-	-		

				6	0.25	659.19	658.95	18.97	18.06	-	-	-	-	-		
23	09-16/09/2016	61474	219	1	0.42	658.83	659.26	13.78	15.73	0.22	**632.77**	**633**	18.46	18.34	71	wheel thread scratsh & wheel flange thickness
				2	0.11	659.02	658.91	14.12	12.97	0.27	**631.54**	**631.8**	17.84	17.87	72	
				3	0.26	659.88	660.15	14.94	14.18	0.96	**630.83**	**630.91**	18.84	18.42	73	
				4	0.12	659.95	659.83	14.97	13.22	0.75	**631.27**	**631.42**	18.3	17.86	74	
				5	0.52	659.04	659.56	15.01	13.23	0.13	**634.26**	**634.4**	17.92	17.96	75	
				6	0.43	658.92	659.36	13.68	12.55	0.19	**633.38**	**633.19**	17.94	18.11	76	
24	14-15/11/2016	76430	109	1	0.11	658.81	658.7	18.71	18.59	-	-	-	-	-		wheel flange thickness
				2	0.05	658.86	658.81	19.16	18.28	-	-	-	-	-		
				3	0.49	660.35	659.86	12.45	17.42	0.65	**629.45**	**628.8**	17.88	18	77	
				4	0.31	660.17	659.86	13.68	16.42	0.27	**629.68**	**629.41**	19.6	19.49	78	
				5	0.19	659.16	658.97	18.65	18.27	-	-	-	-	-		
				6	0.09	658.89	658.8	19.18	18.24	-	-	-	-	-		
25	16-	7862	218	1	0.26	641.	642.11	13.65	13.97	0.12	**618.1**	**618**	18.0	18.	79	wheel

	18/11/2016	4				85					**2**		8	17		flange thickness
				2	0.12	642.28	642.16	14.71	14.09	0.06	**616.53**	**616.59**	20.35	19.53	80	
				3	0.16	612.41	612.25	19.62	19.74	0.16	**612.41**	**612.25**	19.62	19.74	81	
				4	0.32	637.64	637.96	13.25	13.07	0.18	**609.91**	**609.73**	17.89	18.05	82	
				5	0.04	626.7	626.74	20.9	20.87	0.04	**626.7**	**626.74**	20.9	20.87	83	
				6	0.13	647.16	647.03	14.81	14.29	0.11	**626.16**	**626.05**	17.99	17.93	84	
26	19to21/11/2016	66522	216	1	0.15	648.92	649.07	16.52	16.1	0.3	**623.18**	**623.48**	20	20.09	85	wheel flange thickness
				2	0.07	645.61	645.54	15.96	15.02	0	**622.13**	**622.13**	18.46	18.4	86	
				3	0.07	660.03	659.96	17.86	16.84	-	-	-	-	-		
				4	0.15	659.99	659.84	18.15	17.53	-	-	-	-	-		
				5	0.08	647.3	647.22	18.47	16.75	0.05	**627.07**	**627.02**	19.69	19.12	87	
				6	0.06	647.24	647.3	16.6	14.75	0.01	**625**	**624.99**	18.38	18.36	88	
27	24/11/2016	26848	211	1	-	-	-	-	-	-	-	-	-	-	-	scratch on thread and
				2	-	-	-	-	-	-	-	-	-	-	-	
				3	0.06	639.74	639.8	18.86	17.79	0.09	630.25	630.25	19.12	19.3	89	

				4	0.42	634.87	635.29	19.28	18.19	0.2	629.22	629.42	18.16	18.15	90	abnormal wheel flange profile
				5	-	-	-	-	-	-	-	-	-	-	-	
				6	-	-	-	-	-	-	-	-	-	-	-	
28			217	1	0.06	651.32	651.26	15.26	15.04	0.11	625.02	625.13	19.14	19.36	91	wheel flange thickness
				2	0.01	654.81	654.82	17.26	16.56	0.07	625.34	625.41	20.76	20.74	92	
				3	0.37	640.7	641.07	17.08	16.19	0.02	616.36	616.34	19.46	19.61	93	
				4	0.2	640.46	640.66	14.77	13.67	0.33	614.21	614.54	18.18	18.31	94	
				5	0.36	659.25	659.61	18.39	18.23	0.22	642.37	642.59	20.91	20.84	95	
				6	0.03	659.23	659.26	17.59	15.38	0.14	641.21	641.36	18.53	18.44	96	
29	30/11/2016	690644	115	1	0.37	659.14	658.77	21.41	19.37	-	-	-	-	-		wheel flange thickness
				2	0.06	659.12	659.06	21.15	19.99	-	-	-	-	-		
				3	4.69	635.12	635.91	19.34	15.24	0.32	607.06	607.58	19.63	19.55	97	
				4	0.45	634.9	635.35	18.52	14.09	0.02	605.31	605.33	18.78	18.71	98	
				5	0.23	659.25	659.02	21.45	20.51	-	-	-	-	-		
				6	0.16	658.	658.66	20.98	19.82	-	-	-	-	-		

						82										
30	12/5/2016	57012	220	1	0	659.3	659.3	18.42	17.65	-	-	-	-	-		wheel flange thickness
				2	0.03	659.72	659.3	17.82	16.97	-	-	-	-	-		
				3	0.22	659.89	660.11	17.64	15.57	0	636.33	636.33	19.69	19.83	99	
				4	0.1	659.82	659.92	18.55	18.69	0	636.29	636.29	18.55	18.69	100	
				5	0.33	658.98	659.31	18.23	17.66	-	-	-	-	-		
				6	0.02	659.12	659.1	18.34	16.64	-	-	-	-	-		
31	13-14/12/2016		219	1	0.22	632.52	632.74	20.21	19.32	-	-	-	-	-		scratch on wheel thread
				2	0.23	631.31	631.54	19.67	19.2	-	-	-	-	-		
				3	0.11	630.62	630.73	20.43	19.41	0.07	626.67	626.6	19.34	19.36	101	
				4	0.16	631.11	631.27	19.88	19.85	0.04	628.28	628.32	19.42	19.48	102	
				5	0.02	634.04	634.02	19.75	18.92	-	-	-	-	-		
				6	0.45	633.21	632.76	19.45	19.17	-	-	-	-	-		
32	15-20/12/20	52732	108	1	0.43	659.65	659.23	21.29	20.63	0.01	653.12	653.13	21.54	21.61	103	scratch on

	16			2	0.04	659.25	659.29	20.87	19.87	0.12	653.12	653.24	20.67	20.74	104	wheel thread
				3	0.73	654.36	655.09	18.78	18.65	-	-	-	-	-		
				4	0.43	653.65	654.04	18.6	18.04	-	-	-	-	-		
				5	0.32	659.5	659.18	20.71	19.97	-	-	-	-	-		
				6	0.31	659.48	659.17	20.98	20.43	-	-	-	-	-		
33	22-28/12/2016	75028	206	1	0.07	648.45	648.52	17.08	16.77	0.02	625.49	625.48	20.46	20.34	105	wheel flange thickness
				2	0.06	647.39	647.45	16.57	15.74	0.05	623.99	623.93	19.81	19.69	106	
				3	0.15	638.77	638.92	15.41	15.38	0.23	615.7	615.47	19.21	19.21	107	
				4	0.23	637.33	637.56	14.6	14.34	0.02	615.31	615.29	18.44	18.28	108	
				5	0.14	652.58	652.72	16.52	16.09	0.0.15	625.91	626.06	20.72	20.44	109	
				6	0.23	652.36	652.59	16.07	15.47	0.33	625.06	624.73	19.94	19.91	110	

APPENDEX C

列车转向架数据数据Bogie wheel flange thickness

CAR ID	A车1轴A axle 1		A车2轴A axle 2		B车3轴B axle 3		B车4轴B axle 4		C车5轴C axle 5		C车6轴C axle 6		运行公里数 Operating km	测量人 operator	作业时间 Date	备注 Remark
	左L	右R	左L	右R	左L	右R	左L	右R	左L	右R	左L	右R				
210	28.50	28.50	26.60	28.40	27.60	28.30	27.30	27.10	29.00	28.50	27.40	28.00	35955		4/10/2016	
203	33.20	33.30	33.20	33.10	33.20	33.00	33.00	33.10	33.40	33.10	33.00	33.10	113		4/12/2016	
213	27.20	26.10	24.00	27.90	26.70	28.70	26.60	27.20	27.50	26.20	26.00	28.10	43247		4/7/2016	
217	26.90	26.50	27.00	28.10	25.90	27.00	23.90	24.00	28.90	28.10	26.20	27.90	32603		4/7/2016	
218	29.50	26.10	25.70	26.90	27.10	30.50	25.30	26.40	27.80	29.90	27.10	29.50	38498		4/9/2016	
219	29.10	27.10	26.90	26.60	26.70	28.90	26.50	27.40	26.90	27.80	26.40	26.40	38066		4/9/2016	
205	28.70	29.30	25.00	29.80	30.00	29.80	28.90	28.40	28.00	28.40	29.80	30.00	39118		4/7/2016	
215	28.40	27.60	26.60	28.50	26.80	25.90	24.50	26.10	26.00	26.80	26.60	26.80	44988		4/7/2016	
209	28.90	27.80	28.20	28.40	29.20	29.20	28.00	27.80	28.70	28.30	28.60	27.50	46240		4/10/2016	
208	27.30	29.90	28.50	29.60	27.90	28.20	28.80	27.50	30.20	25.20	29.10	27.40	33022			

206	29.60	29.20	27.50	29.30	26.80	27.60	27.30	26.40	28.80	29.60	28.00	29.80			4/11/2016	
211	28.70	29.10	26.90	27.30	27.30	28.80	22.20	29.90	28.90	29.10	25.70	28.90	26848		4/7/2016	
212	29.10	27.50	25.00	28.40	28.80	27.30	28.50	28.80	30.60	27.00	28.30	28.00	41732		4/8/2016	

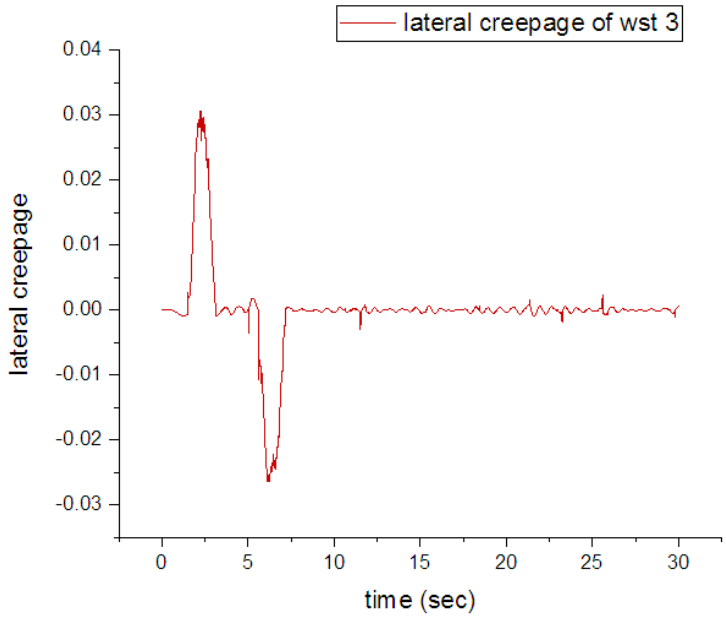
lateral creepage of wst 3
lateral creepage
0.04
0.03
0.02
0.01
0.00
-0.01
-0.02
-0.03
0
5
10
15
20
25
30
time (sec)

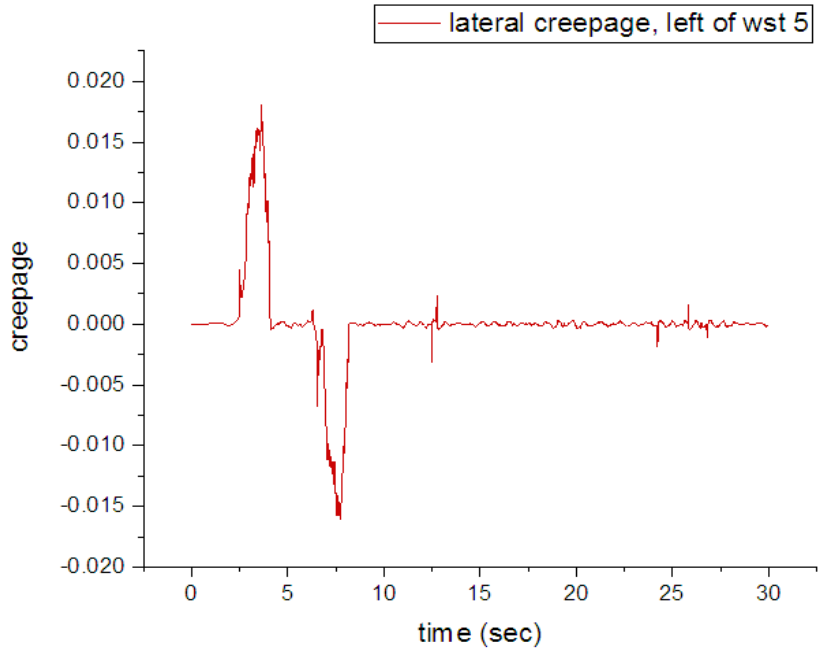
lateral creepage, left of wst 5
creepage
0.020
0.015
0.010
0.005
0.000
-0.005
-0.010
-0.015
-0.020
0
5
10
15
20
25
30
time (sec)

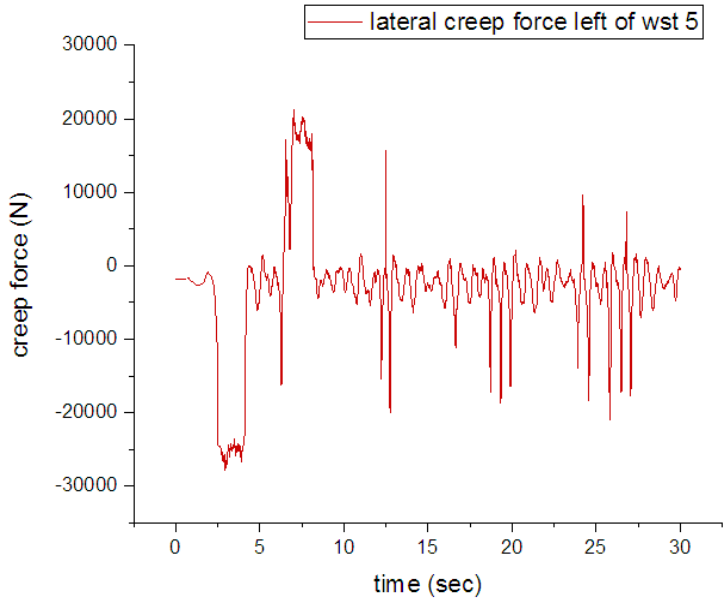
lateral creep force left of wst 5
creep force (N)
30000
20000
10000
0
-10000
-20000
-30000
0
5
10
15
20
25
30
time (sec)

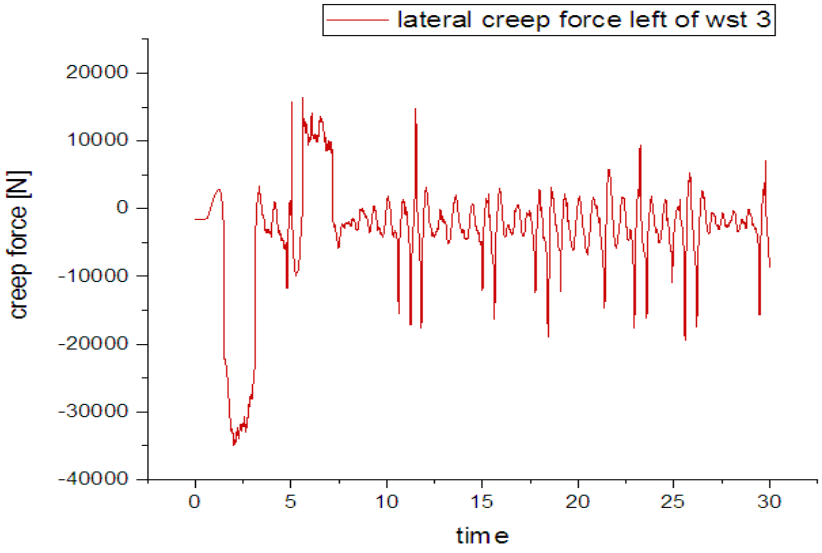
lateral creep force left of wst 3
creep force [N]
20000
10000
0
-10000
-20000
-30000
-40000
0
5
10
15
20
25
30
time

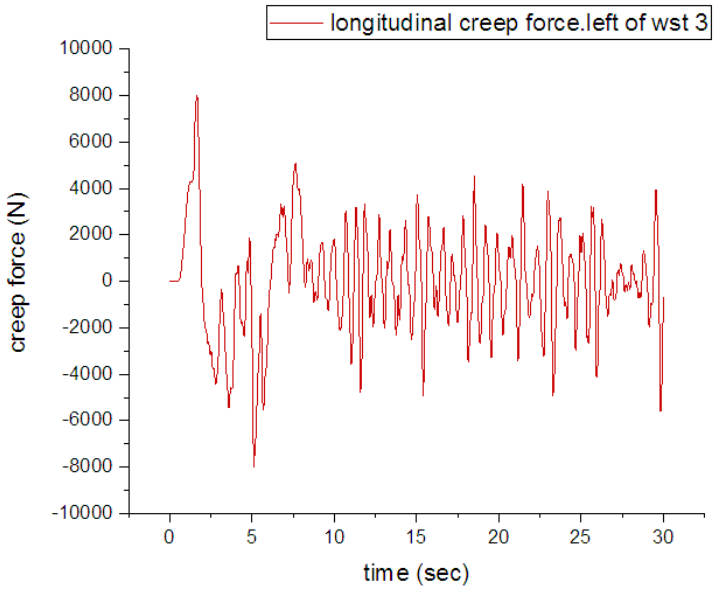
longitudinal creep force.left of wst 3
creep force (N)
10000
8000
6000
4000
2000
0
-2000
-4000
-6000
-8000
-10000
0
5
10
15
20
25
30
time (sec)

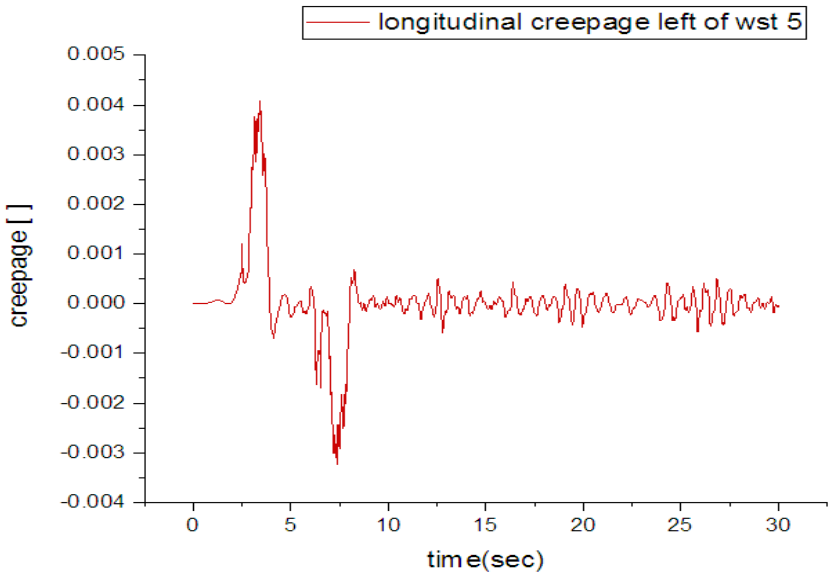
longitudinal creepage left of wst 5
creepage [ ]
0.005
0.004
0.003
0.002
0.001
0.000
-0.001
-0.002
-0.003
-0.004
0
5
10
15
20
25
30
time(sec)

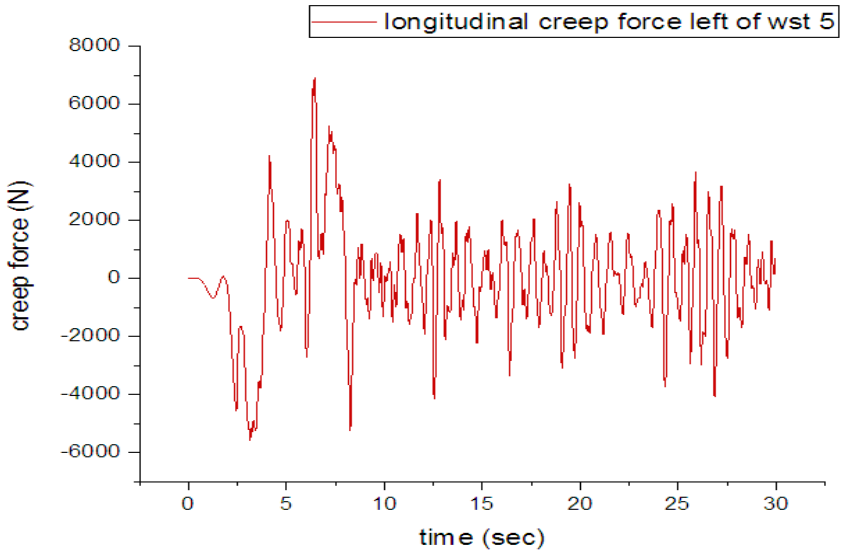
longitudinal creep force left of wst 5
creep force (N)
8000
6000
4000
2000
0
-2000
-4000
-6000
0
5
10
15
20
25
30
time (sec)